

1 Quasi-consistent efficient meshfree thin shell
2 formulation to naturally accommodate essential
3 boundary conditions

4 Junchao Wu^{a,*}, Yangtao Xu^b, Bin Xu^a, Syed Humayun Basha^{c,*}

^a*Key Laboratory for Intelligent Infrastructure and Monitoring of Fujian Province, College
of Civil Engineering, Huaqiao University, Xiamen, Fujian, 361021, China*

^b*College of Civil Engineering, Huaqiao University, Xiamen, Fujian, 361021, China*

^c*Key Laboratory for Structural Engineering and Disaster Prevention of Fujian Province,
College of Civil Engineering, Huaqiao University, Xiamen, Fujian, 361021, China*

5 **Abstract**

This research proposed an efficient and quasi-consistent meshfree thin shell formulation with natural enforcement of essential boundary conditions. Within the framework of the Hu-Washizu variational principle, a mixed formulation of displacements, strains and stresses is employed in this approach, where the displacements are discretized using meshfree shape functions, and the strains and stresses are expressed using smoothed gradients, covariant smoothed gradients and covariant bases. The smoothed gradients satisfy the first and second order integration constraint and have quasi-consistent consistency. Owing to Hu-Washizu variational principle, the essential boundary conditions automatically arise in its weak form. As a result, the suggested technique's enforcement of essential boundary conditions resembles that of the traditional Nitsche's method. Contrary to Nitsche's method, the costly higher order derivatives of conventional meshfree shape functions were replaced by the smoothed gradients with fast computation, which improve the efficiency. Meanwhile, the proposed formulation features a naturally stabilized term without adding any artificial stabilization factors, which eliminates the stabilization parameter-dependent issue in the Nitsche's method. The efficacy of the proposed Hu-Washizu meshfree thin shell formulation is illustrated by a set of classical standard thin shell problems.

6 *Keywords:* Meshfree, Thin shell, Hu-Washizu variational principle,
7 Reproducing kernel gradient smoothing, Essential boundary condition

*Corresponding author

Email addresses: jcwu@hqu.edu.cn (Junchao Wu), syedhbasha@hqu.edu.cn (Syed Humayun Basha)

8 1. Introduction

9 Thin shell structures generally adhere to the Kirchhoff hypothesis [1], that
10 neglects the shear deformation can be described using Galerkin formulation
11 which requires to have at least C^1 continuity. The traditional finite element
12 methods usually only have C^0 continuous shape functions, and it prefers Mindlin
13 thick shear theory, hybrid and mixed models in simulation of shell structure [2].
14 Meshfree methods [3, 4, 5] with high order smoothed shape functions have gar-
15 nered much research attention over the past thirty years. These techniques
16 established the shape functions based on a collection of dispersed nodes, and
17 the high order continuity of shape functions can be easily achieved even with
18 low-order basis functions. For thin shell analysis, this high order meshfree ap-
19 proximation can also alleviate the membrane locking caused by the mismatched
20 approximation order of membrane strain and bending strain [6]. Furthermore,
21 nodal-based meshfree approximations generally offer the flexibility of local re-
22 finement and can relieve the burden of mesh distortion. Owing to these benefits,
23 numerous meshfree techniques have been developed and implemented in many
24 scientific and engineering fields [7, 8, 9, 10, 11, 12]. However, the high order
25 smoothed meshfree shape functions accompany the enlarged and overlapping
26 supports, which may potentially cause many problems for shape functions. One
27 of the issues is the loss of the Kronecker delta property, which means that, un-
28 like the finite element methods, the necessary boundary conditions cannot be
29 directly enforced [13]. Another issue is that the variational consistency or said
30 integration constraint cannot be satisfied due to the misalignment between the
31 numerical integration domains and supports of shape functions. Besides, the
32 shape functions exhibit a piecewise rational nature in each integration domain.
33 Therefore, variational consistency is vital to the solution accuracy in Galerkin
34 formulations [14, 15].

35 Various ways have been presented to enforce the necessary boundary for
36 Galerkin meshfree methods directly, including the boundary singular kernel
37 method [16], mixed transformation method [16], and interpolation element-free
38 method [17] for recovering shape functions' Kronecker property. However, these
39 methods are not based on a variational setting and cannot guarantee varia-
40 tional consistency. In the absence of a meshfree node, accuracy enforcement
41 might be poorer. In contrast, enforcing the essential boundary conditions using
42 a variational approach is preferred for Galerkin meshfree methods. The varia-
43 tional consistent Lagrange multiplier approach was initially used to the Galerkin
44 meshfree method by Belytschko et al. [3]. In this method, the extra degrees
45 of freedom are used to determine the discretion of Lagrange multiplier. Fur-
46 thermore, Ivannikov et al. [18] have extended this approach to geometrically
47 nonlinear thin shells. Lu et al. [19] suggested the modified variational es-
48 sential boundary enforcement approach and expressed the Lagrange multiplier
49 by equivalent tractions to eliminate the excess degrees of freedom. However,
50 the coercivity of this approach is not always ensured and potentially reduces
51 the accuracy. Zhu and Atluri [20] pioneered the penalty method for meshfree
52 method, making it a straightforward approach to enforce essential boundary

53 conditions via Galerkin weak form. However, the penalty method lacks varia-
 54 tional consistency and requires experimental artificial parameters whose optimal
 55 value is hard to determine. Fernández-Méndez and Huerta [13] imposed neces-
 56 sary boundary conditions using Nitsche’s approach in the meshfree formulation.
 57 This approach can be seen as a hybrid combination of the modified variational
 58 method and the penalty method because the modified variational method gen-
 59 erates variational consistency through the use of a consistent term, and the
 60 penalty method is used as a stabilized term to recover the coercivity. Skatulla
 61 and Sansour [21] extended Nitsche’s thin shell analysis method and proposed an
 62 iteration algorithm to determine artificial parameters at each integration point.

63 In order to address the issue of numerical integration, a series of consis-
 64 tent integration schemes have been developed for Galerkin meshfree methods.
 65 Among these include stabilized conforming nodal integration [22], variational
 66 consistent integration [23], quadratic consistent integration [24], reproducing
 67 kernel gradient smoothing integration [25], and consistent projection integration
 68 [26]. The assumed strain approach establishes the most consistent integration
 69 scheme, while the smoothed gradient replaces the costly higher order derivatives
 70 of traditional meshfree shape functions and shows a high efficiency. Moreover,
 71 to achieve global variational consistency, a consistent essential boundary con-
 72 dition enforcement should cooperate with the consistent integration scheme.
 73 The consistent integration scheme and Nitsche’s method for treating essential
 74 boundary conditions show a good performance since they can satisfy the coer-
 75 civity without requiring additional degrees of freedom. Nevertheless, Nitsche’s
 76 approach still retains the artificial parameters in stabilized terms, and it is es-
 77 sential to remain conscious of the costly higher order derivatives, particularly
 78 for thin plate and thin shell problems. Recently, Wu et al. [27, 28] proposed
 79 an efficient and stabilized essential boundary condition enforcement method
 80 based upon the Hellinger-Reissner variational principle, where a mixed formu-
 81 lation in Hellinger-Reissner weak form recasts the reproducing kernel gradient
 82 smoothing integration. The terms for enforcing essential boundary conditions
 83 are identical to the Nitsche’s method, and both have consistent and stabilized
 84 terms. Nevertheless, the stabilized term of this method naturally exists in the
 85 Hellinger-Reissner weak form and no longer needs the artificial parameters, even
 86 for essential boundary enforcement; instead all of the higher order derivatives
 87 are represented by smoothed gradients and their derivatives.

88 In this study, an efficient and stabilized variational consistent meshfree
 89 method that naturally enforces the essential boundary conditions is developed
 90 for thin shell structure. Following the concept of the Hellinger-Reissner prin-
 91 ciple base consistent meshfree method, the Hu-Washizu variational principle of
 92 complementary energy with variables of displacement, strains, and stresses is
 93 employed. The displacement is approximated by conventional meshfree shape
 94 functions, and the strains and stresses are expressed by smoothed gradients with
 95 covariant bases. It is important to note that although the first second-order in-
 96 tegration requirements are naturally embedded in the smoothed gradients, their
 97 fulfillment can only result in a quasi-satisfaction of variational consistency be-
 98 cause of the non-polynomial nature of the stresses. Hu-Washizu’s weak form is

99 used to evaluate all the essential boundary conditions regarding displacements
100 and rotations. This type of formulation is similar to the Nitsche's method but
101 does not require any artificial parameters. Compared with Nitsche's method,
102 conventional reproducing smoothed gradients and its direct derivatives replace
103 the costly higher order derivatives. By utilizing the advantages of a replicating
104 kernel gradient smoothing framework, the smoothed gradients showed better
105 performance compared to conventional derivatives of shape functions, hence
106 increasing the meshfree formulation's computational efficiency.

107 The remainder of this research paper is structured as follows: The kinematics
108 of the thin shell structure and the weak form of the associated Hu-Washizu
109 principle are briefly described in Section 2. Subsequently, the mixed formulation
110 regarding the displacements, strains and stresses in accordance with Hu-Washizu
111 weak form are presented in Section 3. The discrete equilibrium equations are
112 derived in Section 4 using the naturally occurring accommodation of essential,
113 and they are compared to the equations obtained using Nitsche's method. The
114 numerical results in Section 5 validate the efficacy of the proposed Hu-Washizu
115 meshfree thin shell formulation. Lastly, the concluding remarks are presented
116 in Section 6.

117 2. Hu-Washizu's formulation of complementary energy for thin shell

118 2.1. Kinematics for thin shell

119 Consider the configuration of a shell $\bar{\Omega}$, as shown in Fig. 1, which can be
 120 easily described by a parametric curvilinear coordinate system $\boldsymbol{\xi} = \{\xi^i\}_{i=1,2,3}$.
 121 The mid-surface of the shell denoted by Ω is specified by the in-plane coordinates
 122 $\boldsymbol{\xi} = \{\xi^\alpha\}_{\alpha=1,2}$, as the thickness direction of shell is by ξ^3 , $-\frac{h}{2} \leq \xi^3 \leq \frac{h}{2}$, h is
 123 the thickness of shell. In this work, Latin indices take the values from 1 to 3,
 124 and Greek indices are evaluated by 1 or 2. For the Kirchhoff hypothesis [6], the
 125 position $\mathbf{x} \in \bar{\Omega}$ is defined by linear functions with respect to ξ^3 :

$$\mathbf{x}(\xi^1, \xi^2, \xi^3) = \mathbf{r}(\xi^1, \xi^2) + \xi^3 \mathbf{a}_3(\xi^1, \xi^2) \quad (1)$$

in which \mathbf{r} means the position on the mid-surface of shell, and \mathbf{a}_3 is correspond-

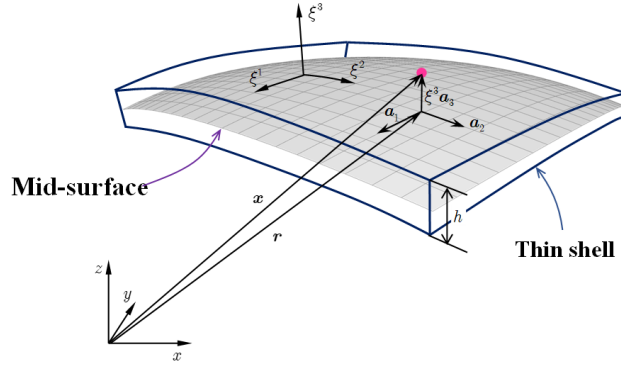


Figure 1: Kinematics for thin shell.

126 ing normal direction. For the mid-surface of shell, the in-plane covariant base
 127 vector with respect to ξ^α can be derived by a trivial partial differentiation to \mathbf{r} :
 128

$$\mathbf{a}_\alpha = \frac{\partial \mathbf{r}}{\partial \xi^\alpha} = \mathbf{r}_{,\alpha}, \alpha = 1, 2 \quad (2)$$

129 to provide for a clear expression, the subscript comma denotes the partial dif-
 130 ferentiation operation with respect to in-plane coordinates ξ^α , and the normal
 131 vector \mathbf{a}_3 can be obtained by the normalized cross product of \mathbf{a}_α 's as follows:

$$\mathbf{a}_3 = \frac{\mathbf{a}_1 \times \mathbf{a}_2}{\|\mathbf{a}_1 \times \mathbf{a}_2\|} \quad (3)$$

132 where $\|\bullet\|$ is the Euclidean norm operator.

133 With the assumption of infinitesimal deformation, the strain components
 134 with respect to the global contravariant base can be stated as:

$$\epsilon_{ij} = \frac{1}{2}(\mathbf{x}_{,i} \cdot \mathbf{u}_{,j} + \mathbf{u}_{,i} \cdot \mathbf{x}_{,j}) \quad (4)$$

where \mathbf{u} represents the displacement for the shell deformation. To satisfy the Kirchhoff hypothesis, the displacement is assumed to be of the following form:

$$\mathbf{u}(\xi^1, \xi^2, \xi^3) = \mathbf{v}(\xi^1, \xi^2) + \boldsymbol{\theta}(\xi^1, \xi^2)\xi^3 \quad (5)$$

in which the quadratic and higher order terms are neglected. \mathbf{v} , $\boldsymbol{\theta}$ represent the displacement and rotation in mid-surface, respectively.

Subsequently, plugging Eqs. (1) and (5) into Eq. (4) and neglecting the quadratic terms, the strain components can be rephrased as follows:

$$\begin{aligned} \epsilon_{\alpha\beta} &= \frac{1}{2}(\mathbf{a}_\alpha \cdot \mathbf{v}_{,\beta} + \mathbf{v}_{,\alpha} \cdot \mathbf{a}_\beta) \\ &\quad + \frac{1}{2}(\mathbf{a}_{3,\alpha} \cdot \mathbf{v}_{,\beta} + \mathbf{v}_{,\alpha} \cdot \mathbf{a}_{3,\beta} + \mathbf{a}_\alpha \cdot \boldsymbol{\theta}_{,\beta} + \boldsymbol{\theta}_{,\alpha} \cdot \mathbf{a}_\beta)\xi^3 \\ &= \varepsilon_{\alpha\beta} + \kappa_{\alpha\beta}\xi^3 \end{aligned} \quad (6a)$$

$$\epsilon_{\alpha 3} = \frac{1}{2}(\mathbf{a}_\alpha \cdot \boldsymbol{\theta} + \mathbf{v}_{,\alpha} \cdot \mathbf{a}_3) + \frac{1}{2}(\mathbf{a}_3 \cdot \boldsymbol{\theta})_{,\alpha}\xi^3 \quad (6b)$$

$$\epsilon_{33} = \mathbf{a}_3 \cdot \boldsymbol{\theta} \quad (6c)$$

where $\varepsilon_{\alpha\beta}$, $\kappa_{\alpha\beta}$ represent membrane and bending strains, respectively, and are given as follows:

$$\varepsilon_{\alpha\beta} = \frac{1}{2}(\mathbf{a}_\alpha \cdot \mathbf{v}_{,\beta} + \mathbf{v}_{,\alpha} \cdot \mathbf{a}_\beta) \quad (7)$$

$$\kappa_{\alpha\beta} = \frac{1}{2}(\mathbf{a}_{3,\alpha} \cdot \mathbf{v}_{,\beta} + \mathbf{v}_{,\alpha} \cdot \mathbf{a}_{3,\beta} + \mathbf{a}_\alpha \cdot \boldsymbol{\theta}_{,\beta} + \boldsymbol{\theta}_{,\alpha} \cdot \mathbf{a}_\beta) \quad (8)$$

In accordance with the Kirchhoff hypothesis, the thickness of shell will not change, and the deformation related with direction of ξ^3 will vanish, i.e. $\epsilon_{3i} = 0$. Thus, the rotation $\boldsymbol{\theta}$ can be rewritten as:

$$\epsilon_{3i} = 0 \Rightarrow \begin{cases} \boldsymbol{\theta} \cdot \mathbf{a}_\alpha + \mathbf{v}_{,\alpha} \cdot \mathbf{a}_3 = 0 \\ \boldsymbol{\theta} \cdot \mathbf{a}_3 = 0 \end{cases} \Rightarrow \boldsymbol{\theta} = -\mathbf{v}_{,\alpha} \cdot \mathbf{a}_3 \mathbf{a}^\alpha \quad (9)$$

where \mathbf{a}^α 's is the in-plane contravariant base vector, $\mathbf{a}^\alpha \cdot \mathbf{a}_\beta = \delta^\alpha_\beta$, δ is the Kronecker delta function. The detailed derivation of Eq. 9 can be found in reference [30].

Furthermore, substituting Eq. (9) into Eq. (8) leads to:

$$\kappa_{\alpha\beta} = (\Gamma_{\alpha\beta}^\gamma \mathbf{v}_{,\gamma} - \mathbf{v}_{,\alpha\beta}) \cdot \mathbf{a}_3 = -\mathbf{v}_{,\alpha}|_\beta \cdot \mathbf{a}_3 \quad (10)$$

in which $\Gamma_{\alpha\beta}^\gamma = \mathbf{a}_{\alpha,\beta} \cdot \mathbf{a}^\gamma$ is namely the Christoffel symbol of the second kind, and $\mathbf{v}_{,\alpha}|_\beta$ is the in-plane covariant derivative of $\mathbf{v}_{,\alpha}$, i.e. $\mathbf{v}_{,\alpha}|_\beta = \Gamma_{\alpha\beta}^\gamma \mathbf{v}_{,\gamma} - \mathbf{v}_{,\alpha\beta}$.

2.2. Galerkin weak form for Hu-Washizu principle of complementary energy

In this study, the Hu-Washizu variational principle of complementary energy [29] was adopted for the development of the proposed analytical approach, the

156 corresponding complementary functional, denoted by Π_C , is listed as follows:

$$\begin{aligned}
& \Pi_C(\varepsilon_{\alpha\beta}, \kappa_{\alpha\beta}, N^{\alpha\beta}, M^{\alpha\beta}) \\
&= \int_{\Omega} \frac{h}{2} \varepsilon_{\alpha\beta} C^{\alpha\beta\gamma\eta} \varepsilon_{\gamma\eta} d\Omega + \int_{\Omega} \frac{h^3}{24} \kappa_{\alpha\beta} C^{\alpha\beta\gamma\eta} \kappa_{\gamma\eta} d\Omega \\
&+ \int_{\Omega} \varepsilon_{\alpha\beta} (N^{\alpha\beta} - h C^{\alpha\beta\gamma\eta} \varepsilon_{\gamma\eta}) d\Omega + \int_{\Omega} \kappa_{\alpha\beta} (M^{\alpha\beta} - \frac{h^3}{12} C^{\alpha\beta\gamma\eta} \kappa_{\gamma\eta}) d\Omega \\
&- \int_{\Gamma_v} \mathbf{T} \cdot \bar{\mathbf{v}} d\Gamma + \int_{\Gamma_{\theta}} M_{\mathbf{n}\mathbf{n}} \bar{\theta}_{\mathbf{n}} d\Gamma - (P \mathbf{a}_3 \cdot \bar{\mathbf{v}})_{\mathbf{x} \in C_w}
\end{aligned} \tag{11}$$

157 where $C^{\alpha\beta\gamma\eta}$'s represent the components of fourth order elasticity tensor with
158 respect to the covariant base and plane stress assumption, and it can be ex-
159 pressed by Young's modulus E , Poisson's ratio ν and the in-plane contravariant
160 metric coefficients $a^{\alpha\beta}$'s, $a^{\alpha\beta} = \mathbf{a}^{\alpha} \cdot \mathbf{a}^{\beta}$, as follows:

$$C^{\alpha\beta\gamma\eta} = \frac{E}{2(1+\nu)} (a^{\alpha\gamma} a^{\beta\eta} + a^{\alpha\eta} a^{\beta\gamma} + \frac{2\nu}{1-\nu} a^{\alpha\beta} a^{\gamma\eta}) \tag{12}$$

161 and $N^{\alpha\beta}$, $M^{\alpha\beta}$ are the components of membrane and bending stresses given by:

$$N^{\alpha\beta} = h C^{\alpha\beta\gamma\eta} \varepsilon_{\gamma\eta}, \quad M^{\alpha\beta} = \frac{h^3}{12} C^{\alpha\beta\gamma\eta} \kappa_{\gamma\eta} \tag{13}$$

162 Essential boundaries on the edges and corners denoted by Γ_v , Γ_{θ} and C_v are
163 naturally existed in complementary energy functional, $\bar{\mathbf{v}}$, $\bar{\theta}_{\mathbf{n}}$ are the correspond-
164 ing prescribed displacement and normal rotation, respectively. \mathbf{T} , $M_{\mathbf{n}\mathbf{n}}$ and P
165 can be determined by Euler-Lagrange equations of shell problem [30] as follows:

$$\mathbf{T} = \mathbf{T}_N + \mathbf{T}_M \rightarrow \begin{cases} \mathbf{T}_N = \mathbf{a}_{\alpha} N^{\alpha\beta} n_{\beta} \\ \mathbf{T}_M = (\mathbf{a}_3 M^{\alpha\beta} s_{\alpha} n_{\beta})_{,\gamma} s^{\gamma} + (\mathbf{a}_3 M^{\alpha\beta})|_{\beta} n_{\alpha} \end{cases} \tag{14}$$

$$M_{\mathbf{n}\mathbf{n}} = M^{\alpha\beta} n_{\alpha} n_{\beta} \tag{15}$$

$$P = -[[M^{\alpha\beta} s_{\alpha} n_{\beta}]] \tag{16}$$

168 where $\mathbf{n} = n^{\alpha} \mathbf{a}_{\alpha} = n_{\alpha} \mathbf{a}^{\alpha}$ and $\mathbf{s} = s^{\alpha} \mathbf{a}_{\alpha} = s_{\alpha} \mathbf{a}^{\alpha}$ are the outward normal and
169 tangent directions on boundaries. $[[f]]$ is the jump operator defined by:

$$[[f]]_{\mathbf{x}=\mathbf{x}_c} = \lim_{\epsilon \rightarrow 0^+} (f(\mathbf{x}_c + \epsilon) - f(\mathbf{x}_c - \epsilon)), \mathbf{x}_c \in \Gamma \tag{17}$$

170 where f is an arbitrary function on Γ .

171 Moreover, the natural boundary conditions should be applied by Lagrangian
172 multiplier method with displacement \mathbf{v} regarded as multiplier. Thus, then the
173 new complementary energy functional namely Π is given by:

$$\begin{aligned}
& \Pi(\mathbf{v}, \varepsilon_{\alpha\beta}, \kappa_{\alpha\beta}, N^{\alpha\beta}, M^{\alpha\beta}) \\
&= \Pi_C(\varepsilon_{\alpha\beta}, \kappa_{\alpha\beta}, N^{\alpha\beta}, M^{\alpha\beta}) + \int_{\Gamma_M} \theta_{\mathbf{n}} (M_{\mathbf{n}\mathbf{n}} - \bar{M}_{\mathbf{n}\mathbf{n}}) d\Gamma \\
&- \int_{\Gamma_T} \mathbf{v} \cdot (\mathbf{T} - \bar{\mathbf{T}}) d\Gamma - \mathbf{v} \cdot \mathbf{a}_3 (P - \bar{P})_{\mathbf{x} \in C_P} - \int_{\Omega} \mathbf{v} \cdot (\mathbf{b} - \bar{\mathbf{b}}) d\Omega
\end{aligned} \tag{18}$$

174 where $\bar{\mathbf{T}}$, \bar{M}_{nn} and \bar{P} are the prescribed traction, bending moment and concen-
 175 trated force on edges Γ_T , Γ_M and corner C_P respectively. All the boundaries
 176 meet the following geometric relationships:

$$\begin{cases} \Gamma = \Gamma_v \cup \Gamma_T \cup \Gamma_\theta \cup \Gamma_M, & C = C_v \cup C_P, \\ \Gamma_v \cap \Gamma_T = \Gamma_\theta \cap \Gamma_M = C_v \cap C_P = \emptyset \end{cases} \quad (19)$$

177 and $\bar{\mathbf{b}}$ stands for the prescribed body force in Ω , \mathbf{b} also can be written based on
 178 Euler-Lagrange equations [30] as:

$$\mathbf{b} = \mathbf{b}_N + \mathbf{b}_M \rightarrow \begin{cases} \mathbf{b}_N = (\mathbf{a}_\alpha N^{\alpha\beta})|_\beta \\ \mathbf{b}_M = (\mathbf{a}_3 M^{\alpha\beta})|_{\alpha\beta} \end{cases} \quad (20)$$

179 Introducing a standard variational argument to Eq. (18), $\delta\Pi = 0$, and
 180 considering the arbitrariness of virtual variables, $\delta\mathbf{v}$, $\delta\varepsilon_{\alpha\beta}$, $\delta\kappa_{\alpha\beta}$, $N^{\alpha\beta}$, $M^{\alpha\beta}$
 181 lead to the following weak form:

$$-\int_{\Omega} h\delta\varepsilon_{\alpha\beta} C^{\alpha\beta\gamma\eta} \varepsilon_{\gamma\eta} d\Omega + \int_{\Omega} \delta\varepsilon_{\alpha\beta} N^{\alpha\beta} d\Omega = 0 \quad (21a)$$

$$-\int_{\Omega} \frac{h^3}{12} \delta\kappa_{\alpha\beta} C^{\alpha\beta\gamma\eta} \kappa_{\gamma\eta} d\Omega + \int_{\Omega} \delta\kappa_{\alpha\beta} M^{\alpha\beta} d\Omega = 0 \quad (21b)$$

$$\begin{aligned} \int_{\Omega} \delta N^{\alpha\beta} \varepsilon_{\alpha\beta} d\Omega - \int_{\Gamma} \delta \mathbf{T}_N \cdot \mathbf{v} d\Gamma + \int_{\Omega} \delta \mathbf{b}_N \cdot \mathbf{v} d\Omega \\ + \int_{\Gamma_v} \delta \mathbf{T}_N \cdot \mathbf{v} d\Gamma = \int_{\Gamma_v} \delta \mathbf{T}_N \cdot \bar{\mathbf{v}} d\Gamma \end{aligned} \quad (21c)$$

$$\begin{aligned} \int_{\Omega} \delta M^{\alpha\beta} \kappa_{\alpha\beta} d\Omega - \int_{\Gamma} \delta M_{nn} \theta_n d\Gamma + \int_{\Gamma} \delta \mathbf{T}_M \cdot \mathbf{v} d\Gamma + (\delta P \mathbf{a}_3 \cdot \mathbf{v})_{\mathbf{x} \in C} + \int_{\Omega} \delta \mathbf{b}_M \cdot \mathbf{v} d\Omega \\ + \int_{\Gamma_\theta} \delta M_{nn} \theta_n d\Gamma - \int_{\Gamma_v} \delta \mathbf{T}_M \cdot \mathbf{v} d\Gamma - (\delta P \mathbf{a}_3 \cdot \mathbf{v})_{\mathbf{x} \in C_v} \\ = \int_{\Gamma_\theta} \delta M_{nn} \bar{\theta}_n d\Gamma - \int_{\Gamma_v} \delta \mathbf{T}_M \cdot \bar{\mathbf{v}} d\Gamma - (\delta P \mathbf{a}_3 \cdot \bar{\mathbf{v}})_{\mathbf{x} \in C_v} \end{aligned} \quad (21d)$$

$$\begin{aligned} \int_{\Gamma} \delta \theta_n M_{nn} d\Gamma - \int_{\Gamma} \delta \mathbf{v} \cdot \mathbf{T} d\Gamma - (\delta \mathbf{v} \cdot \mathbf{a}_3 P)_{\mathbf{x} \in C} + \int_{\Omega} \delta \mathbf{v} \cdot \mathbf{b} d\Omega \\ - \int_{\Gamma_\theta} \delta \theta_n M_{nn} d\Gamma + \int_{\Gamma_v} \delta \mathbf{v} \cdot \mathbf{T} d\Gamma + (\delta \mathbf{v} \cdot \mathbf{a}_3 P)_{\mathbf{x} \in C_v} = - \int_{\Gamma_T} \delta \mathbf{v} \cdot \bar{\mathbf{t}} d\Gamma - \int_{\Omega} \delta \mathbf{v} \cdot \bar{\mathbf{b}} d\Omega \end{aligned} \quad (21e)$$

186 where the geometric relationships of Eq. (19) is used herein.

187 3. Mixed meshfree formulation for modified Hellinger-Reissner weak 188 form

189 3.1. Reproducing kernel approximation for displacement

190 This study approximates the displacement by adopting reproducing kernel
191 approximation. As shown in Fig. 2, the mid-surface of the shell Ω is discretized
192 by a set of meshfree nodes $\{\boldsymbol{\xi}_I\}_{I=1}^{n_p}$ in parametric configuration, where n_p is the
193 total number of meshfree nodes. The approximated displacement namely \boldsymbol{v}^h
194 can be expressed as:

$$\boldsymbol{v}(\boldsymbol{\xi}) = \sum_{I=1}^{n_p} \Psi_I(\boldsymbol{\xi}) \boldsymbol{d}_I \quad (22)$$

195 in which Ψ_I and \boldsymbol{d}_I is the shape function and nodal coefficient tensor related by
196 node $\boldsymbol{\xi}_I$. According to reproducing kernel approximation [4], the shape function
197 takes the following form:

$$\Psi_I(\boldsymbol{\xi}) = \boldsymbol{p}^T(\boldsymbol{\xi}) \boldsymbol{c}(\boldsymbol{\xi}) \phi(\boldsymbol{\xi}_I - \boldsymbol{\xi}) \quad (23)$$

198 where \boldsymbol{p} is the basis function vector represented using the following quadratic
199 function as:

$$\boldsymbol{p} = \{1, \xi^1, \xi^2, (\xi^1)^2, \xi^1 \xi^2, (\xi^2)^2\}^T \quad (24)$$

200 The kernel function denoted by ϕ controls the support and smoothness of
201 meshfree shape functions. The quintic B-spline function with square support is
202 used herein as the kernel function:

$$\phi(\boldsymbol{\xi}_I - \boldsymbol{\xi}) = \phi(\hat{s}_1) \phi(\hat{s}_2), \quad \hat{s}_\alpha = \frac{|\xi_I^\alpha - \xi^\alpha|}{s_{\alpha I}} \quad (25)$$

203 with

$$\phi(\hat{s}_\alpha) = \frac{1}{5!} \begin{cases} (3 - 3\hat{s}_\alpha)^5 - 6(2 - 3\hat{s}_\alpha)^5 + 15(1 - 3\hat{s}_\alpha)^5 & \hat{s}_\alpha \leq \frac{1}{3} \\ (3 - 3\hat{s}_\alpha)^5 - 6(2 - 3\hat{s}_\alpha)^5 & \frac{1}{3} < \hat{s}_\alpha \leq \frac{2}{3} \\ (3 - 3\hat{s}_\alpha)^5 & \frac{2}{3} < \hat{s}_\alpha \leq 1 \\ 0 & \hat{s}_\alpha > 1 \end{cases} \quad (26)$$

204 and $\hat{s}_{\alpha I}$ means the characterized size of support for meshfree shape function Ψ_I .

205 The unknown vector \boldsymbol{c} in shape function are determined by the fulfillment
206 of the so-called consistency condition:

$$\sum_{I=1}^{n_p} \Psi_I(\boldsymbol{\xi}) \boldsymbol{p}(\boldsymbol{\xi}_I) = \boldsymbol{p}(\boldsymbol{\xi}) \quad (27)$$

207 or equivalently

$$\sum_{I=1}^{n_p} \Psi_I(\boldsymbol{\xi}) \boldsymbol{p}(\boldsymbol{\xi}_I - \boldsymbol{\xi}) = \boldsymbol{p}(\mathbf{0}) \quad (28)$$

208 Substituting Eq. (22) into (28), yields:

$$\mathbf{A}(\boldsymbol{\xi})\mathbf{c}(\boldsymbol{\xi}) = \mathbf{p}(\mathbf{0}) \quad \Rightarrow \quad \mathbf{c}(\boldsymbol{\xi}) = \mathbf{A}^{-1}(\boldsymbol{\xi})\mathbf{p}(\mathbf{0}) \quad (29)$$

209 where \mathbf{A} is the moment matrix:

$$\mathbf{A}(\boldsymbol{\xi}) = \sum_{I=1}^{n_p} \phi(\boldsymbol{\xi}_I - \boldsymbol{\xi}) \mathbf{p}(\boldsymbol{\xi}_I - \boldsymbol{\xi}) \mathbf{p}^T(\boldsymbol{\xi}_I - \boldsymbol{\xi}) \quad (30)$$

210 Substituting Eq. (29) back into Eq. (22), the expression of meshfree shape
211 function can be written as:

$$\Psi_I(\boldsymbol{\xi}) = \mathbf{p}^T(\boldsymbol{\xi}_I - \boldsymbol{\xi}) \mathbf{A}^{-1}(\boldsymbol{\xi}) \mathbf{p}(\mathbf{0}) \phi(\boldsymbol{\xi}_I - \boldsymbol{\xi}) \quad (31)$$

212 3.2. Reproducing kernel gradient smoothing approximation for effective stress 213 and strain

214 In Galerkin meshfree formulation, the mid-plane of thin shell Ω is split by
215 a set of integration cells Ω_C 's, $\cup_{C=1}^{n_e} \Omega_C \approx \Omega$, as shown in Fig. 2. With the
216 inspiration of reproducing kernel smoothing framework, the Cartesian and co-
217 variant derivatives of displacement, $\mathbf{v}_{,\alpha}$ and $-\mathbf{v}_{,\alpha}|_{\beta}$, in strains $\varepsilon_{\alpha\beta}$, $\kappa_{\alpha\beta}$ are
218 approximated by $(p-1)$ -th order polynomials in each integration cells. In inte-
219 gration cell Ω_C , the approximated derivatives and strains denoted by $\mathbf{v}_{,\alpha}^h$, $\varepsilon_{\alpha\beta}^h$
220 and $-\mathbf{v}_{,\alpha}^h|_{\beta}$, $\kappa_{\alpha\beta}^h$ can be expressed by:

$$\mathbf{v}_{,\alpha}^h(\boldsymbol{\xi}) = \mathbf{q}^T(\boldsymbol{\xi}) \mathbf{d}_{\alpha}^{\varepsilon}, \quad \varepsilon_{\alpha\beta}^h(\boldsymbol{\xi}) = \mathbf{q}^T(\boldsymbol{\xi}) \frac{1}{2} (\mathbf{a}_{\alpha} \cdot \mathbf{d}_{\beta}^{\varepsilon} + \mathbf{a}_{\beta} \cdot \mathbf{d}_{\alpha}^{\varepsilon}) \quad (32)$$

$$-\mathbf{v}_{,\alpha}^h|_{\beta}(\boldsymbol{\xi}) = \mathbf{q}^T(\boldsymbol{\xi}) \mathbf{d}_{\alpha\beta}^{\kappa}, \quad \kappa_{\alpha\beta}^h(\boldsymbol{\xi}) = \mathbf{q}^T(\boldsymbol{\xi}) \mathbf{a}_3 \cdot \mathbf{d}_{\alpha\beta}^{\kappa} \quad (33)$$

222 where \mathbf{q} is the linear polynomial vector and has the following form:

$$\mathbf{q} = \{1, \xi^1, \xi^2\}^T \quad (34)$$

223 and the $\mathbf{d}_{\alpha}^{\varepsilon}$, $\mathbf{d}_{\alpha\beta}^{\kappa}$ are the corresponding coefficient vector tensors. For the con-
224 ciseness, the mixed usage of tensor and vector is introduced in this study. For
225 instance, the component of coefficient tensor vector $\mathbf{d}_{\alpha I}^{\varepsilon}$, $\mathbf{d}_{\alpha}^{\varepsilon} = \{\mathbf{d}_{\alpha I}^{\varepsilon}\}$, is a three
226 dimensional tensor, $\dim \mathbf{d}_{\alpha I}^{\varepsilon} = \dim \mathbf{v}$.

227 In order to meet the integration constraint of thin shell problem, the ap-
228 proximated stresses $N^{\alpha\beta h}$, $M^{\alpha\beta h}$ are assumed to be a similar form with strains,
229 yields:

$$N^{\alpha\beta h}(\boldsymbol{\xi}) = \mathbf{q}^T(\boldsymbol{\xi}) \mathbf{a}^{\alpha} \cdot \mathbf{d}_N^{\beta}, \quad \mathbf{a}_{\alpha} N^{\alpha\beta h}(\boldsymbol{\xi}) = \mathbf{q}^T(\boldsymbol{\xi}) \mathbf{d}_N^{\beta} \quad (35)$$

$$M^{\alpha\beta h}(\boldsymbol{\xi}) = \mathbf{q}^T(\boldsymbol{\xi}) \mathbf{a}_3 \cdot \mathbf{d}_M^{\alpha\beta}, \quad \mathbf{a}_3 M^{\alpha\beta h}(\boldsymbol{\xi}) = \mathbf{q}^T(\boldsymbol{\xi}) \mathbf{d}_M^{\alpha\beta} \quad (36)$$

231 substituting the approximations of Eqs. (22), (32), (33), (35), (36) into Eqs.
232 (21c), (21d) can express $\mathbf{d}_{\beta}^{\varepsilon}$ and $\mathbf{d}_{\alpha\beta}^{\kappa}$ by \mathbf{d} as:

$$\mathbf{d}_{\beta}^{\varepsilon} = \mathbf{G}^{-1} \left(\sum_{I=1}^{n_p} (\tilde{\mathbf{g}}_{\beta I} - \bar{\mathbf{g}}_{\beta I}) \mathbf{d}_I + \hat{\mathbf{g}}_{\beta} \right) \quad (37)$$

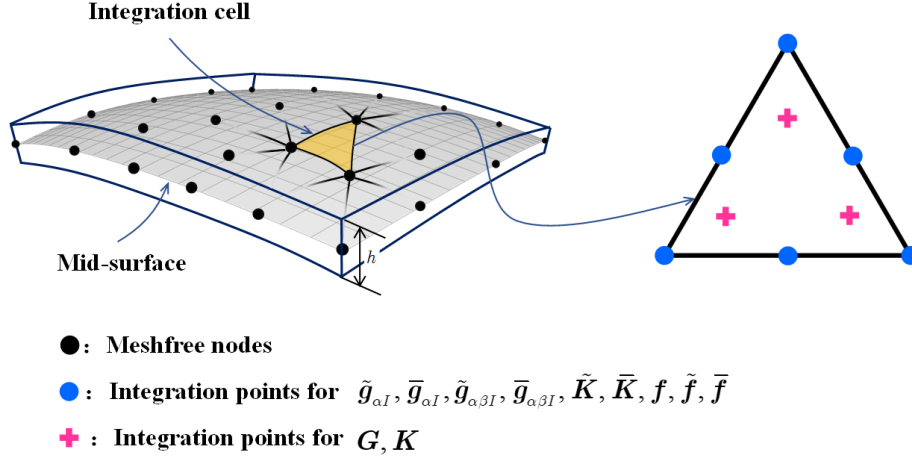


Figure 2: Integration scheme for Hu-Washizu weak form.

$$d_{\alpha\beta}^{\kappa} = G^{-1} \left(\sum_{I=1}^{n_p} (\tilde{g}_{\alpha\beta I} - \bar{g}_{\alpha\beta I}) d_I + \hat{g}_{\alpha\beta} \right) \quad (38)$$

with

$$G = \int_{\Omega_C} q^T q d\Omega \quad (39)$$

$$\tilde{g}_{\beta I} = \int_{\Gamma_C} \Psi_I q n_{\beta} d\Gamma - \int_{\Omega_C} \Psi_I q_{|\beta} d\Omega \quad (40a)$$

$$\bar{g}_{\beta I} = \int_{\Gamma_C \cap \Gamma_v} \Psi_I q n_{\beta} d\Gamma \quad (40b)$$

$$\hat{g}_{\beta} = \int_{\Gamma_C \cap \Gamma_v} q n_{\beta} \bar{v} d\Gamma \quad (40c)$$

$$\begin{aligned} \tilde{g}_{\alpha\beta I} = & \int_{\Gamma_C} \Psi_{I,\gamma} n^{\gamma} q n_{\alpha} n_{\beta} d\Gamma - \int_{\Gamma_C} \Psi_I (q_{|\beta} n_{\alpha} + (q s_{\alpha} n_{\beta})_{,\gamma} s^{\gamma}) d\Gamma \\ & + [[\Psi_I q s_{\alpha} n_{\beta}]]_{\mathbf{x} \in C_C} - \int_{\Omega_C} \Psi q_{,\alpha|\beta} d\Omega \end{aligned} \quad (41a)$$

$$\begin{aligned} \bar{g}_{\alpha\beta I} = & \int_{\Gamma_C \cap \Gamma_{\theta}} \Psi_{I,\gamma} n^{\gamma} q n_{\alpha} n_{\beta} d\Gamma - \int_{\Gamma_C \cap \Gamma_v} \Psi_I (q_{|\beta} n_{\alpha} + (q s_{\alpha} n_{\beta})_{,\gamma} s^{\gamma}) d\Gamma \\ & + [[\Psi_I q s_{\alpha} n_{\beta}]]_{\mathbf{x} \in C_C \cap C_v} \end{aligned} \quad (41b)$$

$$\begin{aligned} \hat{g}_{\alpha\beta} = & \int_{\Gamma_C \cap \Gamma_{\theta}} q n_{\alpha} n_{\beta} a_3 \bar{\theta}_{\mathbf{n}} d\Gamma - \int_{\Gamma_C \cap \Gamma_v} (q_{|\beta} n_{\alpha} + (q s_{\alpha} n_{\beta})_{,\gamma} s^{\gamma}) \bar{v} d\Gamma \\ & + [[q s_{\alpha} n_{\beta} \bar{v}]]_{\mathbf{x} \in C_C \cap C_v} \end{aligned} \quad (41c)$$

where evaluations of $\mathbf{q}_{|\beta}$, $\mathbf{q}_{,\alpha|\beta}$ are detail in Appendix A. Further plugging Eqs. (37) and (38) back into Eqs. (32) and (33) respectively gives the final expression of $\mathbf{v}_{,\alpha}^h$, $\varepsilon_{\alpha\beta}^h$ and $-\mathbf{v}_{,\alpha\beta}^h$, $\kappa_{\alpha\beta}^h$ as:

$$\mathbf{v}_{,\alpha}^h = \sum_{I=1}^{n_p} (\tilde{\Psi}_{I,\alpha} - \bar{\Psi}_{I,\alpha}) \mathbf{d}_I + \mathbf{q}^T \mathbf{G}^{-1} \hat{\mathbf{g}}_\alpha \quad (42a)$$

$$\begin{aligned} \varepsilon_{\alpha\beta}^h &= \sum_{I=1}^{n_p} \frac{1}{2} (\mathbf{a}_\alpha \tilde{\Psi}_{I,\beta} + \mathbf{a}_\beta \tilde{\Psi}_{I,\alpha}) \cdot \mathbf{d}_I - \sum_{I=1}^{n_p} \frac{1}{2} (\mathbf{a}_\alpha \bar{\Psi}_{I,\beta} + \mathbf{a}_\beta \bar{\Psi}_{I,\alpha}) \cdot \mathbf{d}_I \\ &\quad + \mathbf{q}^T \mathbf{G}^{-1} \frac{1}{2} (\mathbf{a}_\alpha \cdot \hat{\mathbf{g}}_\beta + \mathbf{a}_\beta \cdot \hat{\mathbf{g}}_\alpha) \\ &= \tilde{\varepsilon}_{\alpha\beta}^h - \bar{\varepsilon}_{\alpha\beta}^h + \hat{\varepsilon}_{\alpha\beta}^h \end{aligned} \quad (42b)$$

$$-\mathbf{v}_{,\alpha\beta}^h = \sum_{I=1}^{n_p} (\tilde{\Psi}_{I,\alpha\beta} - \bar{\Psi}_{I,\alpha\beta}) \mathbf{d}_I + \mathbf{q}^T \mathbf{G}^{-1} \hat{\mathbf{g}}_{\alpha\beta} \quad (43a)$$

$$\begin{aligned} \kappa_{\alpha\beta}^h &= \sum_{I=1}^{n_p} \tilde{\Psi}_{I,\alpha\beta} \mathbf{a}_3 \cdot \mathbf{d}_I - \sum_{I=1}^{n_p} \bar{\Psi}_{I,\alpha\beta} \mathbf{a}_3 \cdot \mathbf{d}_I + \mathbf{q}^T \mathbf{G}^{-1} \mathbf{a}_3 \cdot \hat{\mathbf{g}}_{\alpha\beta} \\ &= \tilde{\kappa}_{\alpha\beta}^h - \bar{\kappa}_{\alpha\beta}^h + \hat{\kappa}_{\alpha\beta}^h \end{aligned} \quad (43b)$$

with

$$\begin{cases} \tilde{\varepsilon}_{\alpha\beta}^h = \sum_{I=1}^{n_p} \frac{1}{2} (\mathbf{a}_\alpha \tilde{\Psi}_{I,\beta} + \mathbf{a}_\beta \tilde{\Psi}_{I,\alpha}) \cdot \mathbf{d}_I = \sum_{I=1}^{n_p} \tilde{\varepsilon}_{\alpha\beta I} \cdot \mathbf{d}_I \\ \bar{\varepsilon}_{\alpha\beta}^h = \sum_{I=1}^{n_p} \frac{1}{2} (\mathbf{a}_\alpha \bar{\Psi}_{I,\beta} + \mathbf{a}_\beta \bar{\Psi}_{I,\alpha}) \cdot \mathbf{d}_I = \sum_{I=1}^{n_p} \bar{\varepsilon}_{\alpha\beta I} \cdot \mathbf{d}_I \\ \hat{\varepsilon}_{\alpha\beta}^h = \mathbf{q}^T \mathbf{G}^{-1} \frac{1}{2} (\mathbf{a}_\alpha \cdot \hat{\mathbf{g}}_\beta + \mathbf{a}_\beta \cdot \hat{\mathbf{g}}_\alpha) \end{cases} \quad (44)$$

$$\begin{cases} \tilde{\Psi}_{I,\alpha}(\boldsymbol{\xi}) = \mathbf{q}^T(\boldsymbol{\xi}) \mathbf{G}^{-1} \tilde{\mathbf{g}}_{\alpha I} \\ \bar{\Psi}_{I,\alpha}(\boldsymbol{\xi}) = \mathbf{q}^T(\boldsymbol{\xi}) \mathbf{G}^{-1} \bar{\mathbf{g}}_{\alpha I} \\ \tilde{\varepsilon}_{\alpha\beta I} = \frac{1}{2} (\mathbf{a}_\alpha \tilde{\Psi}_{I,\beta} + \mathbf{a}_\beta \tilde{\Psi}_{I,\alpha}) \\ \bar{\varepsilon}_{\alpha\beta I} = \frac{1}{2} (\mathbf{a}_\alpha \bar{\Psi}_{I,\beta} + \mathbf{a}_\beta \bar{\Psi}_{I,\alpha}) \end{cases} \quad (45)$$

$$\begin{cases} \tilde{\kappa}_{\alpha\beta}^h = \sum_{I=1}^{n_p} \tilde{\Psi}_{I,\alpha\beta} \mathbf{a}_3 \cdot \mathbf{d}_I = \sum_{I=1}^{n_p} \tilde{\kappa}_{\alpha\beta I} \cdot \mathbf{d}_I \\ \bar{\kappa}_{\alpha\beta}^h = \sum_{I=1}^{n_p} \bar{\Psi}_{I,\alpha\beta} \mathbf{a}_3 \cdot \mathbf{d}_I = \sum_{I=1}^{n_p} \bar{\kappa}_{\alpha\beta I} \cdot \mathbf{d}_I \\ \hat{\kappa}_{\alpha\beta}^h = \mathbf{q}^T \mathbf{G}^{-1} \mathbf{a}_3 \cdot \hat{\mathbf{g}}_{\alpha\beta} \end{cases} \quad (46)$$

$$\begin{cases} \tilde{\Psi}_{I,\alpha\beta}(\boldsymbol{\xi}) = \mathbf{q}^T(\boldsymbol{\xi})\mathbf{G}^{-1}\tilde{\mathbf{g}}_{\alpha\beta I} \\ \bar{\Psi}_{I,\alpha\beta}(\boldsymbol{\xi}) = \mathbf{q}^T(\boldsymbol{\xi})\mathbf{G}^{-1}\tilde{\mathbf{g}}_{\alpha\beta I} \\ \tilde{\boldsymbol{\kappa}}_{\alpha\beta I} = \tilde{\Psi}_{I,\alpha\beta}\mathbf{a}_3 \\ \bar{\boldsymbol{\kappa}}_{\alpha\beta I} = \bar{\Psi}_{I,\alpha\beta}\mathbf{a}_3 \end{cases} \quad (47)$$

247 It has to be noted that, referring to reproducing kernel gradient smoothing
 248 framework [25], $\tilde{\Psi}_{I,\alpha}$, $\tilde{\Psi}_{I,\alpha\beta}$ are actually the first and second order smoothed
 249 gradients in curvilinear coordinates. $\tilde{\mathbf{g}}_{\alpha I}$ and $\tilde{\mathbf{g}}_{\alpha\beta I}$ are the right hand side in-
 250 tegration constraints for first and second order gradients, then this formulation
 251 can meet the variational consistency for the p -th order polynomials. It should
 252 be known that, in curved model, the variational consistency for non-polynomial
 253 functions, like trigonometric functions, should be required for the polynomial
 254 solution. Even with p -th order variational consistency, the proposed formulation
 255 can not exactly reproduce the solution spanned by basis functions. However,
 256 the accuracy of reproducing kernel smoothed gradients is still better than tradi-
 257 tional meshfree formulation. Numerical examples in the section below will pro-
 258 vide better evidence to prove the accuracy of the reproducing kernel smoothed
 259 gradients.

260 **4. Naturally variational enforcement for essential boundary condi-**
 261 **tions**

262 *4.1. Discrete equilibrium equations*

263 With the approximated effective stresses and strains, the last equation of
 264 weak form Eq. (21e) becomes:

$$-\sum_{C=1}^{n_e} \sum_{I=1}^{n_p} \delta \mathbf{d}_I \cdot \left((\tilde{\mathbf{g}}_{\alpha I}^T - \bar{\mathbf{g}}_{\alpha I}^T) \mathbf{d}_N^\alpha + (\tilde{\mathbf{g}}_{\alpha \beta I}^T - \bar{\mathbf{g}}_{\alpha \beta I}^T) \mathbf{d}_M^{\alpha \beta} \right) = -\sum_{I=1}^{n_p} \delta \mathbf{d}_I \cdot \mathbf{f}_I \quad (48)$$

265 where \mathbf{f}_I 's are the components of the traditional force vector:

$$\mathbf{f}_I = \int_{\Gamma_t} \Psi_I \bar{\mathbf{t}} d\Gamma - \int_{\Gamma_M} \Psi_{I,\gamma} n^\gamma \bar{M}_{nn} d\Gamma + [[\Psi_I \mathbf{a}_3 \bar{P}]]_{\mathbf{x} \in C_P} + \int_{\Omega} \Psi_I \bar{\mathbf{b}} d\Omega \quad (49)$$

266 The left side of Eq. (48) can be simplified using the following steps. For clarity,
 267 the derivation of first term in Eq. (48) taken as an example is given by:

$$\begin{aligned} \sum_{I=1}^{n_p} \delta \mathbf{d}_I \cdot \tilde{\mathbf{g}}_{\alpha I}^T \mathbf{d}_N^\alpha &= \sum_{I=1}^{n_p} \delta \mathbf{d}_I \cdot (\mathbf{G}^{-1} \tilde{\mathbf{g}}_{\alpha I})^T \mathbf{G} \mathbf{d}_N^\alpha \\ &= \int_{\Omega_C} \sum_{I=1}^{n_p} \delta \mathbf{d}_I \cdot (\mathbf{q}^T \mathbf{G}^{-1} \tilde{\mathbf{g}}_{\alpha I})^T \mathbf{q}^T \mathbf{d}_N^\alpha d\Omega \\ &= \int_{\Omega_C} \sum_{I=1}^{n_p} \delta \mathbf{d}_I \cdot \mathbf{a}_\beta (\mathbf{q}^T \mathbf{G}^{-1} \tilde{\mathbf{g}}_{\alpha I})^T N^{\alpha \beta h} d\Omega \\ &= \int_{\Omega_C} \delta \tilde{\varepsilon}_{\alpha \beta}^h N^{\alpha \beta h} d\Omega \end{aligned} \quad (50)$$

268 following the above procedure and including the weak form of Eqs. (21a), (21b),
 269 the left side of Eq. (48) in Ω_C becomes:

$$\begin{aligned}
 & \sum_{I=1}^{n_p} \delta \mathbf{d}_I \cdot \left((\tilde{\mathbf{g}}_{\alpha I}^T - \bar{\mathbf{g}}_{\alpha I}^T) \mathbf{d}_N^\alpha + (\tilde{\mathbf{g}}_{\alpha \beta I}^T - \bar{\mathbf{g}}_{\alpha \beta I}^T) \mathbf{d}_M^{\alpha \beta} \right) \\
 &= \int_{\Omega_C} ((\delta \tilde{\varepsilon}_{\alpha \beta}^h - \delta \bar{\varepsilon}_{\alpha \beta}^h) N^{\alpha \beta h} + (\delta \tilde{\kappa}_{\alpha \beta}^h - \delta \bar{\kappa}_{\alpha \beta}^h) M^{\alpha \beta h}) d\Omega \\
 &= \int_{\Omega_C} (\delta \tilde{\varepsilon}_{\alpha \beta}^h - \delta \bar{\varepsilon}_{\alpha \beta}^h) h C^{\alpha \beta \gamma \eta} \varepsilon_{\gamma \eta}^h + (\delta \tilde{\kappa}_{\alpha \beta}^h - \delta \bar{\kappa}_{\alpha \beta}^h) \frac{h^3}{12} C^{\alpha \beta \gamma \eta} \kappa_{\gamma \eta}^h \\
 &= \int_{\Omega_C} \delta \tilde{\varepsilon}_{\alpha \beta}^h h C^{\alpha \beta \gamma \eta} \varepsilon_{\gamma \eta}^h d\Omega + \int_{\Omega_C} \delta \tilde{\kappa}_{\alpha \beta}^h \frac{h^3}{12} C^{\alpha \beta \gamma \eta} \kappa_{\gamma \eta}^h d\Omega \\
 &\quad - \int_{\Omega_C} \delta \bar{\varepsilon}_{\alpha \beta}^h h C^{\alpha \beta \gamma \eta} \varepsilon_{\gamma \eta}^h d\Omega - \int_{\Omega_C} \delta \bar{\kappa}_{\alpha \beta}^h h C^{\alpha \beta \gamma \eta} \kappa_{\gamma \eta}^h d\Omega \\
 &\quad - \int_{\Omega_C} \delta \tilde{\kappa}_{\alpha \beta}^h \frac{h^3}{12} C^{\alpha \beta \gamma \eta} \bar{\kappa}_{\gamma \eta}^h d\Omega - \int_{\Omega_C} \delta \bar{\kappa}_{\alpha \beta}^h \frac{h^3}{12} C^{\alpha \beta \gamma \eta} \tilde{\kappa}_{\gamma \eta}^h d\Omega \\
 &\quad + \int_{\Omega_C} \delta \bar{\varepsilon}_{\alpha \beta}^h h C^{\alpha \beta \gamma \eta} \varepsilon_{\gamma \eta}^h d\Omega + \int_{\Omega_C} \delta \bar{\kappa}_{\alpha \beta}^h \frac{h^3}{12} C^{\alpha \beta \gamma \eta} \bar{\kappa}_{\gamma \eta}^h d\Omega \\
 &\quad + \int_{\Omega_C} (\delta \tilde{\varepsilon}_{\alpha \beta}^h - \delta \bar{\varepsilon}_{\alpha \beta}^h) h C^{\alpha \beta \gamma \eta} \varepsilon_{\gamma \eta}^h d\Omega + \int_{\Omega_C} (\delta \tilde{\kappa}_{\alpha \beta}^h - \delta \bar{\kappa}_{\alpha \beta}^h) \frac{h^3}{12} C^{\alpha \beta \gamma \eta} \kappa_{\gamma \eta}^h d\Omega
 \end{aligned} \tag{51}$$

270 on further substituting Eqs. (44) and (46) into above equation gives the final
 271 discrete equilibrium equations, respectively:

$$(\mathbf{K} + \tilde{\mathbf{K}} + \bar{\mathbf{K}}) \mathbf{d} = \mathbf{f} + \tilde{\mathbf{f}} + \bar{\mathbf{f}} \tag{52}$$

272 where

$$\mathbf{K}_{IJ} = \int_{\Omega} \tilde{\varepsilon}_{\alpha \beta I} h C^{\alpha \beta \gamma \eta} \tilde{\varepsilon}_{\gamma \eta J} d\Omega + \int_{\Omega} \tilde{\kappa}_{\alpha \beta I} \frac{h^3}{12} C^{\alpha \beta \gamma \eta} \tilde{\kappa}_{\alpha \beta J} d\Omega \tag{53}$$

273

$$\begin{aligned}
 \tilde{\mathbf{K}}_{IJ} &= - \int_{\Gamma_v} (\Psi_I \tilde{\mathbf{T}}_{NJ} + \tilde{\mathbf{T}}_{NJ} \Psi_J) d\Gamma \\
 &\quad + \int_{\Gamma_\theta} (\Psi_{I,\gamma} n^\gamma \mathbf{a}_3 \tilde{\mathbf{M}}_{nnJ} + \mathbf{a}_3 \tilde{\mathbf{M}}_{nnI} \Psi_{J,\gamma} n^\gamma) d\Gamma
 \end{aligned} \tag{54a}$$

$$\begin{aligned}
 &\quad + ([[\Psi_I \mathbf{a}_3 \tilde{\mathbf{P}}_J]] + [[\tilde{\mathbf{P}}_I \mathbf{a}_3 \Psi_J]])_{\mathbf{x} \in C_v} \\
 \tilde{\mathbf{f}}_I &= - \int_{\Gamma_v} \tilde{\mathbf{T}}_{NI} \cdot \bar{\mathbf{v}} d\Gamma + \int_{\Gamma_\theta} \tilde{\mathbf{M}}_{nnI} \bar{\theta}_n d\Gamma + [[\tilde{\mathbf{P}}_I \mathbf{a}_3 \cdot \bar{\mathbf{v}}]]_{\mathbf{x} \in C_v}
 \end{aligned} \tag{54b}$$

274

$$\bar{\mathbf{K}}_{IJ} = - \int_{\Gamma_v} \bar{\mathbf{T}}_{MI} \Psi_J d\Gamma + \int_{\Gamma_\theta} \mathbf{a}_3 \bar{\mathbf{M}}_{nnI} \Psi_{J,\gamma} n^\gamma d\Gamma + [[\bar{\mathbf{P}}_I \mathbf{a}_3 \Psi_J]]_{\mathbf{x} \in C_v} \tag{55a}$$

$$\bar{\mathbf{f}}_I = - \int_{\Gamma_v} \bar{\mathbf{T}}_{MI} \cdot \bar{\mathbf{v}} d\Gamma + \int_{\Gamma_\theta} \bar{\mathbf{M}}_{nnI} \bar{\theta}_n d\Gamma + [[\bar{\mathbf{P}}_I \mathbf{a}_3 \cdot \bar{\mathbf{v}}]]_{\mathbf{x} \in C_v} \tag{55b}$$

275 The detailed derivations of Eqs (53)-(55) are listed in the Appendix B. As
 276 shown in these equations, Eq. (53) is the conventional stiffness matrix evaluated
 277 by smoothed gradients $\tilde{\Psi}_{I,\alpha}$, $\tilde{\Psi}_{I,\alpha}|_\beta$, and the Eqs. (54) and (55) contribute for
 278 the enforcement of essential boundary. It should be mentioned that, in accor-
 279 dance with reproducing kernel smoothed gradient framework, the integration
 280 scheme of Eqs. (53-55) should be aligned with the those used in the construc-
 281 tion of smoothed gradients. The integration scheme used for proposed method
 282 is shown in Fig. 2, the detailed positions and weight of integration points can
 283 be found in [31] With a close look at Eqs. (54) and (55), the proposed approach
 284 for enforcing essential boundary conditions show an identical structure with tra-
 285 ditional Nitsche's method, both have the consistent and stabilized terms. So,
 286 the next subsection will review the Nitsche's method and compare it with the
 287 proposed method.

288 4.2. Comparison with Nitsche's method

289 The Nitsche's method for enforcing essential boundaries can be regarded as a
 290 combination of Lagrangian multiplier method and penalty method, in which the
 291 Lagrangian multiplier is represented by the approximated displacement. The
 292 corresponding total potential energy functional Π_P is given by:

$$\begin{aligned}
 \Pi_P(\mathbf{v}) = & \int_{\Omega} \frac{1}{2} \varepsilon_{\alpha\beta} N^{\alpha\beta} d\Omega + \int_{\Omega} \frac{1}{2} \kappa_{\alpha\beta} M^{\alpha\beta} d\Omega \\
 & - \int_{\Gamma_t} \mathbf{v} \cdot \bar{\mathbf{t}} d\Gamma + \int_{\Gamma_M} \mathbf{v}_{,\gamma} n^\gamma \mathbf{a}_3 M_{nn} d\Gamma + (\mathbf{v} \cdot \mathbf{a}_3 P)_{\mathbf{x} \in C_P} - \int_{\Omega} \mathbf{v} \cdot \bar{\mathbf{b}} d\Omega \\
 & - \underbrace{\int_{\Gamma_v} \mathbf{t} \cdot (\mathbf{v} - \bar{\mathbf{v}}) d\Gamma + \int_{\Gamma_\theta} M_{nn} (\theta_n - \bar{\theta}_n) d\Gamma + (P \mathbf{a}_3 \cdot (\mathbf{v} - \bar{\mathbf{v}}))_{\mathbf{x} \in C_v}}_{\text{consistent term}} \quad (56) \\
 & + \underbrace{\frac{\alpha_v}{2} \int_{\Gamma_v} \mathbf{v} \cdot \mathbf{v} d\Gamma + \frac{\alpha_\theta}{2} \int_{\Gamma_\theta} \theta_n^2 d\Gamma + \frac{\alpha_C}{2} (\mathbf{v} \cdot \mathbf{v})_{\mathbf{x} \in C_v}}_{\text{stabilized term}}
 \end{aligned}$$

293 where the consistent term generated from the Lagrangian multiplier method
 294 contributes to enforce the essential boundary, and meet the variational con-
 295 sistency condition. However, the consistent term can not always ensure the
 296 coercivity of stiffness, so the penalty method is introduced to serve as a sta-
 297 bilized term. With a standard variational argument, the corresponding weak

form can be stated as:

$$\begin{aligned}
\delta\Pi_P(\mathbf{v}) &= \int_{\Omega} \delta\varepsilon_{\alpha\beta} N^{\alpha\beta} d\Omega + \int_{\Omega} \delta\kappa_{\alpha\beta} M^{\alpha\beta} d\Omega \\
&\quad - \int_{\Gamma_t} \delta\mathbf{v} \cdot \bar{\mathbf{t}} d\Gamma + \int_{\Gamma_M} \delta\mathbf{v}_{,\gamma} n^{\gamma} \mathbf{a}_3 M_{nn} d\Gamma + (\delta\mathbf{v} \cdot \mathbf{a}_3 P)_{\mathbf{x} \in C_P} - \int_{\Omega} \delta\mathbf{v} \cdot \bar{\mathbf{b}} d\Omega \\
&\quad - \int_{\Gamma_v} \delta\mathbf{v} \cdot \mathbf{t} d\Gamma + \int_{\Gamma_{\theta}} \delta\theta_{\mathbf{n}} M_{nn} d\Gamma + (\mathbf{v} \cdot \mathbf{a}_3 P)_{\mathbf{x} \in C_v} \\
&\quad - \int_{\Gamma_v} \delta\mathbf{t} \cdot (\mathbf{v} - \bar{\mathbf{v}}) d\Gamma + \int_{\Gamma_{\theta}} \delta M_{nn} (\theta_{\mathbf{n}} - \bar{\theta}_{\mathbf{n}}) d\Gamma + (\delta P \mathbf{a}_3 \cdot (\mathbf{v} - \bar{\mathbf{v}}))_{\mathbf{x} \in C_v} \\
&\quad + \alpha_v \int_{\Gamma_v} \delta\mathbf{v} \cdot \mathbf{v} d\Gamma + \alpha_{\theta} \int_{\Gamma_{\theta}} \delta\theta_{\mathbf{n}} \theta_{\mathbf{n}} d\Gamma + \alpha_C (\delta\mathbf{v} \cdot \mathbf{v})_{\mathbf{x} \in C_v} \\
&= 0
\end{aligned} \tag{57}$$

in which α_v , α_{θ} and α_C represent experimental artificial parameters. Further invoking the conventional reproducing kernel approximation of Eq. (22) leads to the following discrete equilibrium equations:

$$\sum_{J=1}^{n_p} (\mathbf{K}_{IJ} + \mathbf{K}_{IJ}^c + \mathbf{K}_{IJ}^s) \mathbf{d}_J = \mathbf{f}_I + \mathbf{f}^c + \mathbf{f}^s \tag{58}$$

where the stiffness \mathbf{K}_{IJ} is identical with Eq. (53). \mathbf{K}_{IJ}^c and \mathbf{K}_{IJ}^s are the stiffness matrices for consistent and stabilized terms, respectively, and have the following form:

$$\begin{aligned}
\mathbf{K}_{IJ}^c &= - \int_{\Gamma_v} (\Psi_I \mathbf{T}_{NJ} + \mathbf{T}_{NJ} \Psi_J) d\Gamma \\
&\quad + \int_{\Gamma_{\theta}} (\Psi_{I,\gamma} n^{\gamma} \mathbf{a}_3 \mathbf{M}_{nnJ} + \mathbf{a}_3 \mathbf{M}_{nnI} \Psi_{I,\gamma} n^{\gamma}) d\Gamma \\
&\quad + ([\Psi_I \mathbf{a}_3 \mathbf{P}_J] + [\mathbf{P}_I \mathbf{a}_3 \Psi_J])_{\mathbf{x} \in C_v}
\end{aligned} \tag{59a}$$

$$\mathbf{f}_I^c = - \int_{\Gamma_v} \mathbf{T}_I \cdot \bar{\mathbf{v}} d\Gamma + \int_{\Gamma_{\theta}} \mathbf{M}_{nnI} \bar{\theta}_{\mathbf{n}} d\Gamma + [\mathbf{P}_I \mathbf{a}_3 \cdot \bar{\mathbf{v}}]_{\mathbf{x} \in C_v} \tag{59b}$$

$$\mathbf{K}_{IJ}^s = \alpha_v \int_{\Gamma_v} \Psi_I \Psi_J \mathbf{1} d\Gamma + \alpha_{\theta} \int_{\Gamma_{\theta}} \Psi_{I,\eta} n^{\eta} \mathbf{a}_3 \mathbf{a}_3 n^{\gamma} \Psi_{J,\gamma} d\Gamma + \alpha_C [\Psi_I \mathbf{a}_3 \mathbf{a}_3 \Psi_J]_{\mathbf{x} \in C_v} \tag{60a}$$

$$\mathbf{f}_I^s = \alpha_v \int_{\Gamma_v} \Psi_I \bar{\mathbf{v}} d\Gamma + \alpha_{\theta} \int_{\Gamma_{\theta}} \Psi_{I,\eta} n^{\eta} \mathbf{a}_3 \bar{\theta}_{\mathbf{n}} d\Gamma + \alpha_C [\Psi_I \mathbf{a}_3 \mathbf{a}_3 \cdot \bar{\mathbf{v}}]_{\mathbf{x} \in C_v} \tag{60b}$$

On comparing with the consistent terms of Eqs. (54) and (59), the expressions were almost identical, the major difference is that the higher order derivatives of shape functions have been replaced by smoothed gradients. Owing to

309 the reproducing kernel framework, the construction of smoothed gradients only
310 concerned about the computation of traditional meshfree shape functions and
311 their first order derivatives, which avoid the costly computation of higher order
312 derivatives. Moreover, the stabilized terms in Eq. (60) employs the penalty
313 method to ensure the coercivity of stiffness. In contrast, the stabilized term of
314 Eq. (55) naturally exists in its weak form, and can stabilize the result without
315 considering any artificial parameters.

316 5. Numerical examples

317 The suggested method, which uses Nitsche's method, the consistent repro-
 318 ducing kernel gradient smoothing integration scheme (RKGSI), and the non-
 319 consistent Gauss integration scheme (GI) with penalty method, as well as the
 320 proposed Hu-Washizu formulation (HW) to enforce the necessary boundary con-
 321 ditions, is validated in this section through several examples. A normalized
 322 support size of 2.5 is used for all the methods to ensure the requirement of
 323 quadratic base meshfree approximation. To eliminate the influence of integra-
 324 tion, the Gauss integration scheme uses 6 Gauss points for domain integration
 325 and 3 points for boundary integration, so as to maintain the same integration
 326 accuracy between domain and boundaries. Moreover, the number of integra-
 327 tion points are identical between the Gauss and RKGSI schemes. The error
 328 estimates of displacement (L_2 -Error) and energy (H_e -Error) is used here:

$$\begin{aligned}
 L_2\text{-Error} &= \frac{\sqrt{\int_{\Omega} (\mathbf{v} - \mathbf{v}^h) \cdot (\mathbf{v} - \mathbf{v}^h) d\Omega}}{\sqrt{\mathbf{v} \cdot \mathbf{v}}} \\
 H_e\text{-Error} &= \frac{\sqrt{\int_{\Omega} \left((\varepsilon_{\alpha\beta} - \varepsilon_{\alpha\beta}^h)(N^{\alpha\beta} - N^{\alpha\beta h}) + \int_{\Omega} (\kappa_{\alpha\beta} - \kappa_{\alpha\beta}^h)(M^{\alpha\beta} - M^{\alpha\beta h}) \right) d\Omega}}{\sqrt{\int_{\Omega} (\varepsilon_{\alpha\beta} N^{\alpha\beta} + \kappa_{\alpha\beta} M^{\alpha\beta}) d\Omega}}
 \end{aligned}
 \tag{61}$$

329 5.1. Patch tests

330 The linear and quadratic patch tests for flat and curved thin shells are firstly
 331 studied to verify the variational consistency of the proposed method. As shown
 332 in Fig. 3, the flat and curved models are depicted by an identical parametric
 333 domain $\Omega = (0, 1) \otimes (0, 1)$, where the cylindrical coordinate system with radius
 334 $R = 1$ is employed to describe the curved model, and the whole domain Ω
 335 is discretized by the 165 meshfree nodes. All the boundaries are enforced as
 336 essential boundary conditions with the following manufactured exact solution:

$$\mathbf{v} = \begin{Bmatrix} (\xi^1 + 2\xi^2)^n \\ (3\xi^1 + 4\xi^2)^n \\ (5\xi^1 + 6\xi^2)^n \end{Bmatrix}, \quad n = \begin{cases} 1 & \text{Linear patch test} \\ 2 & \text{Quadratic patch test} \end{cases}
 \tag{62}$$

337 Table 1 lists the L_2 - and H_e -Error results of patch test with flat model, where
 338 the RKGSI scheme with variational consistent essential boundary enforcement,
 339 i.e. RKGSI-Nitsche and RKGSI-HW, can pass the linear and quadratic patch
 340 test. Due to the loss of variational consistency condition, even with Nitsche's
 341 method, Gauss meshfree formulations show noticeable errors. Table 2 shows
 342 the results for curved model, which indicated that all the considered methods
 343 cannot pass the patch test. This is mainly because the proposed smoothed
 344 gradient of Eqs. (35) and (36) could not exactly reproduce the non-polynomial
 345 membrane and bending stress. However, the RKGSI-HW and RKGSI-Nitsche
 346 methods also provide better accuracy compared to others due to the fulfillment

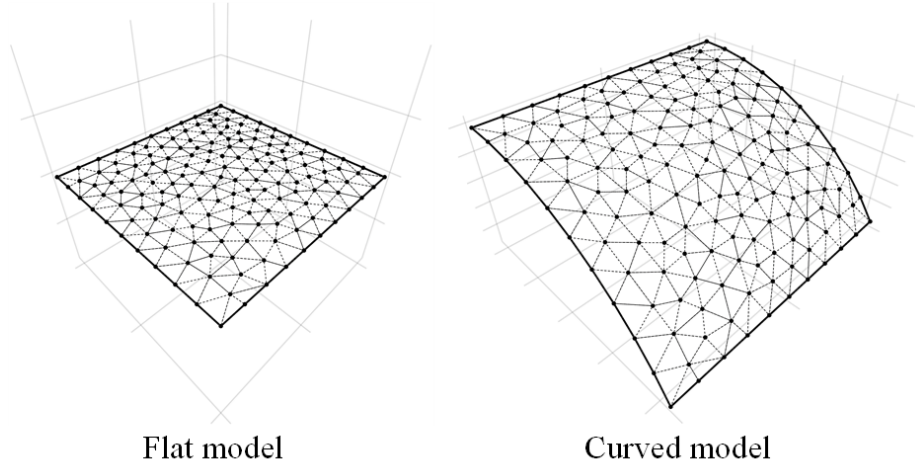


Figure 3: Meshfree discretization for patch test

347 of first second-order variational consistency. Meanwhile, the bending moment
 348 contours of M^{12} are listed in Fig. 4, which further verify that the proposed
 349 method provided a satisfactory result compared to exact solution. On the other
 350 hand, the conventional Gauss meshree formulations showed errors.

Table 1: Results of patch test for flat model.

	Linear patch test		Quadratic patch test	
	L_2 -Error	H_e -Error	L_2 -Error	H_e -Error
GI-Penalty	$4.45E-4$	$1.35E-2$	$2.01E-3$	$1.63E-2$
GI-Nitsche	$4.51E-4$	$1.42E-2$	$1.22E-3$	$1.68E-2$
RKGSi-Penalty	$3.64E-9$	$6.77E-8$	$4.54E-9$	$6.57E-8$
RKGSi-Nitsche	$3.31E-12$	$1.34E-11$	$5.98E-12$	$1.21E-11$
RKGSi-HR	$6.67E-13$	$1.50E-11$	$1.07E-12$	$1.26E-11$

Table 2: Results of patch test for cylindrical model.

	Linear patch test		Quadratic patch test	
	L_2 -Error	H_e -Error	L_2 -Error	H_e -Error
GI-Penalty	$3.79E-4$	$1.30E-2$	$1.74E-3$	$1.37E-2$
GI-Nitsche	$4.04E-4$	$1.42E-2$	$1.15E-3$	$1.49E-2$
RKGSi-Penalty	$1.47E-4$	$5.39E-3$	$2.26E-4$	$2.09E-3$
RKGSi-Nitsche	$2.41E-6$	$7.37E-5$	$2.47E-6$	$2.89E-5$
RKGSi-HR	$4.28E-6$	$1.30E-4$	$9.69E-6$	$2.41E-4$

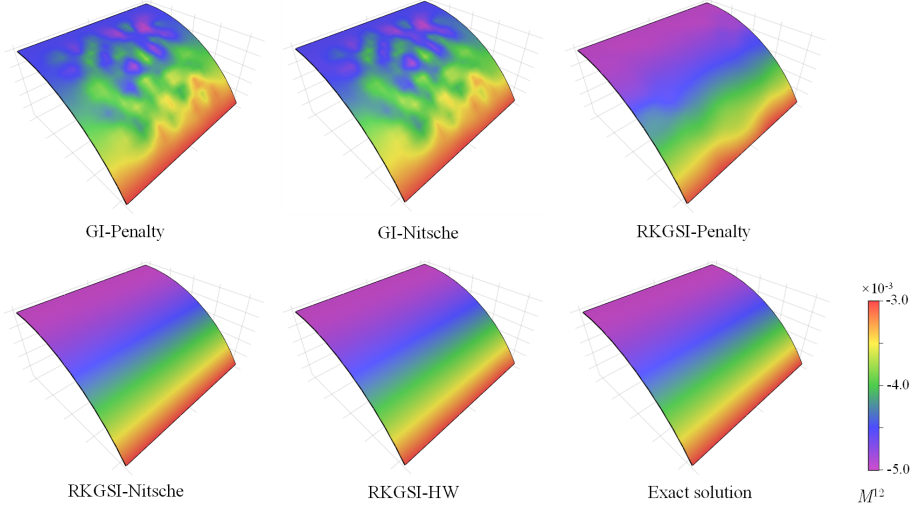


Figure 4: Contour plots of M^{12} for curved shell patch test.

5.2. Scordelis-Lo roof

This example considers the classical Scordelis-Lo roof problem, as depicted in Fig. 5. The cylindrical roof has dimensions $R = 25$, $L = 50$, $h = 0.25$, Young's modulus $E = 4.32 \times 10^8$ and Poisson's ratio $\nu = 0.0$. The entire roof is subjected to a uniform body force of $b_z = -90$, with the straight edges remaining free and the curved edges are enforced by $v_x = v_z = 0$.

Due to the symmetry, only a quadrant of the model is considered for meshfree analysis, which is discretized by the 11×16 , 13×20 , 17×24 and 19×28 meshfree nodes, as listed in Fig. 6. The comparison of the displacement in z -direction at node A , v_{A3} , is used as the investigated quantity, with the reference value 0.3024 given by [32]. Firstly, Fig. 7 presents a sensitivity study for the artificial parameters of α_v 's, α_θ 's in the RKGSI meshfree formulations with Nitsche's method and penalty method. The results of Fig. 7 revealed, Nitsche's method observed less artificial sensitivity. However, both the methods cannot trivially determine the optimal values of the artificial parameters. The optimal artificial parameters from Fig. 7 are adopted for the convergence study in Fig. 8. The convergence result showed that the RKGSI get satisfactory results while the traditional Gauss methods demonstrated noticeable errors.

5.3. Pinched Hemispherical shell

Consider the hemispherical shell shown in Fig. 9, which is loaded at four points $P = \pm 2$ at 90° interval at its bottom. The hemispherical shell has a radius $R = 10$, thickness $h = 0.04$, Young's modulus $E = 6.825 \times 10^7$ and Poisson's ratio $\nu = 0.3$.

Due to symmetry, only quadrant model, where the 8×8 , 16×16 , 24×24 and 32×32 meshfree nodes have been discretized, was considered. The quantity

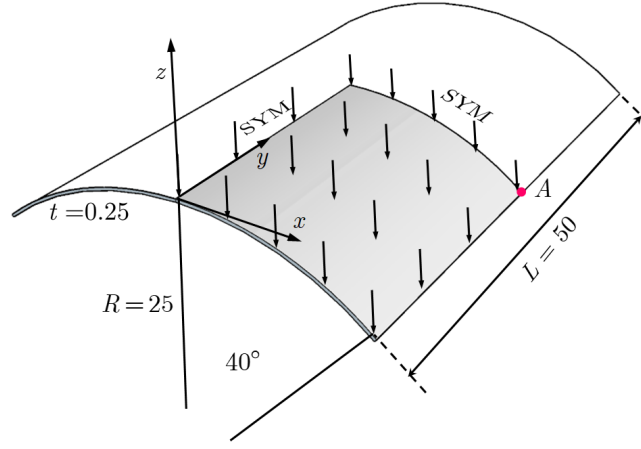


Figure 5: Description of Scordelis-Lo roof problem.

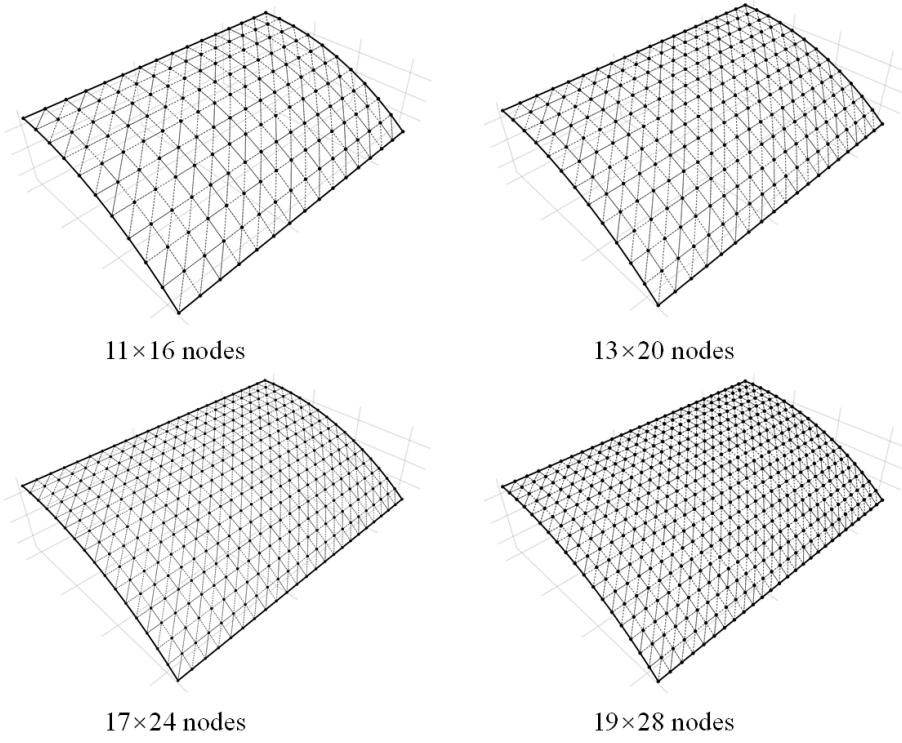


Figure 6: Meshfree discretizations for Scordelis-Lo roof problem.

under investigation for convergence is the displacement at x -direction on point

377 A, v_{A1} . Fig. 10 displays the corresponding convergence results, indicating the
 378 RKGSi scheme performed significantly better compared to the GI meshfree for-
 379 mulation. Meanwhile, the efficiency comparison for this problem is also shown
 380 in Fig. 11, in which the CPU time for assembly and calculation of shape func-
 381 tions are considered. Fig. 11(a) indicates that the RKGSi scheme observed
 382 high efficiency in assembly. This is due to the variational inconsistent Gauss
 383 meshfree formulation which require more Gaussian points to get satisfactory
 384 results. Fig. 11(b) lists the CPU time spent on enforcing essential boundary
 385 conditions for the penalty method, Nitsche's method and proposed HW method.
 386 The results highlighted that the proposed HW method consumed comparable
 387 CPU time in assembly compared to Nitsche's method. However, less time was
 388 spent to calculate the shape functions. Since both the HW method and penalty
 389 method were developed considering the shape functions first order derivatives.
 390 For this reason, both the methods shared an almost identical time in computing
 391 the shape functions.

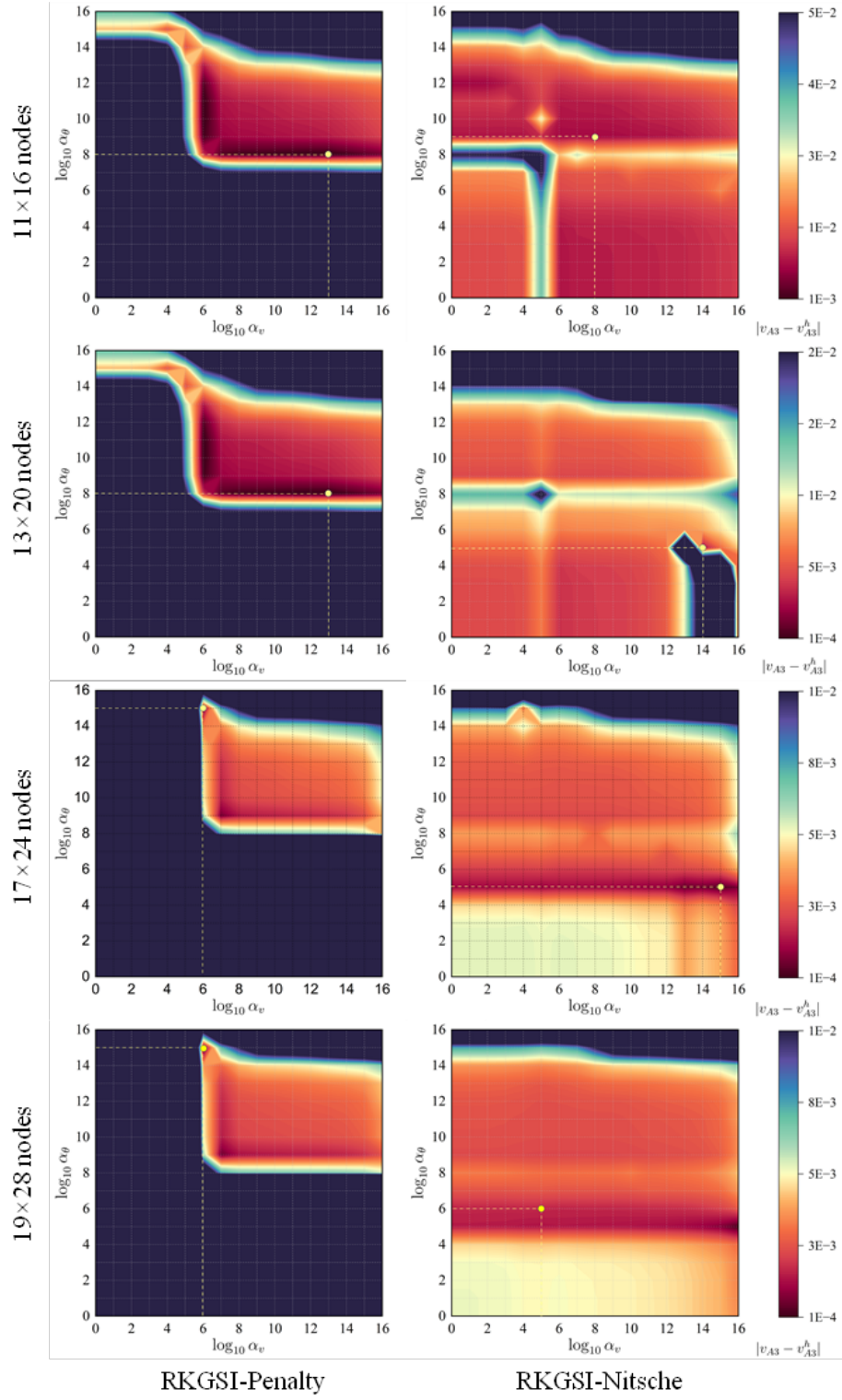


Figure 7: Sensitivity comparison of α_v and α_θ for Scordelis-Lo problem.

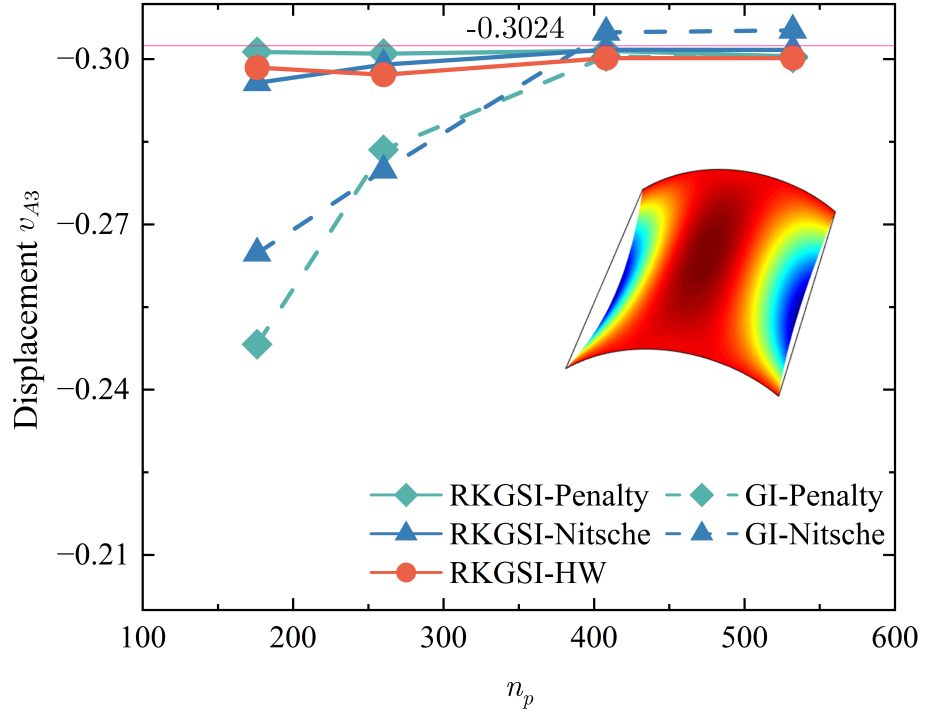


Figure 8: Displacement convergence for Scordelis-Lo roof problem.

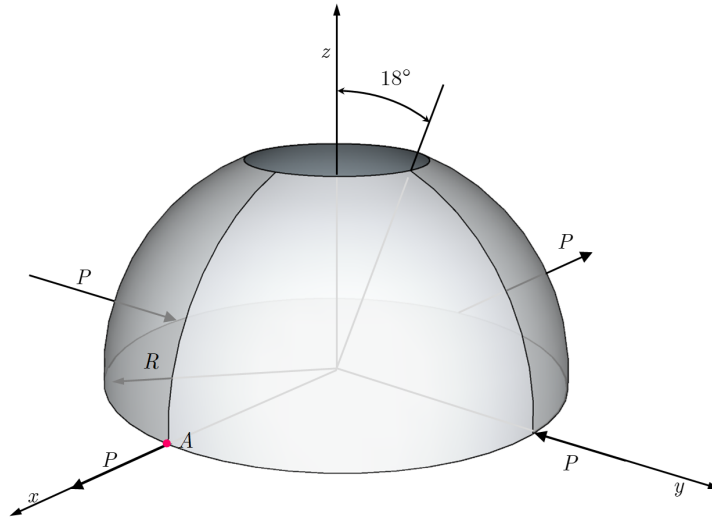


Figure 9: Description of pinched hemispherical shell problem.

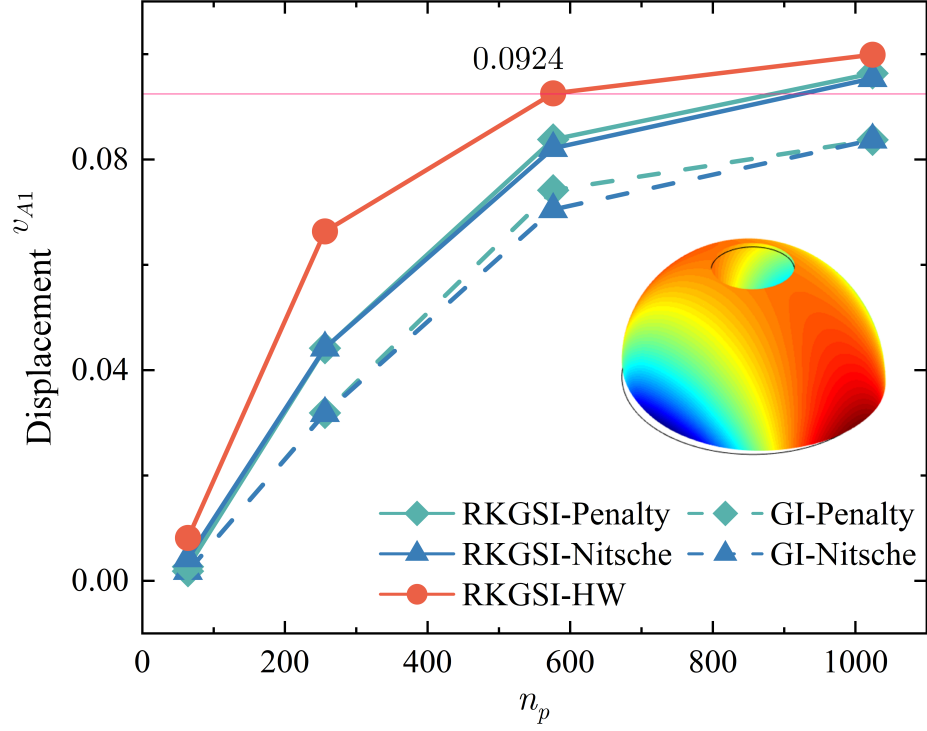


Figure 10: Displacement convergence for pinched hemispherical shell problem.

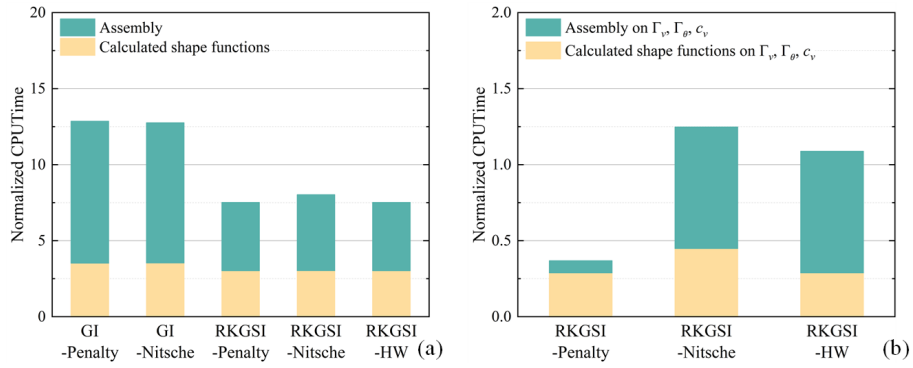


Figure 11: efficiency comparison for pinched hemispherical shell problem: (a) Whole domain; (b) Essential boundaries

6. Conclusion

In this study, an efficient and quasi-consistent meshfree thin shell formulation was presented to naturally enforce the essential boundary conditions. Mixed formulation with the Hu-Washizu principle weak form is adopted, where the traditional meshfree shape functions discretized the displacement, and the strains and stresses were expressed by the reproducing kernel smoothed gradients and the covariant smoothed gradients, respectively. The smoothed gradient naturally embedded the first second-order integration constraints and has a quasi variational consistency for the curved models in each integration cell. Owing to the Hu-Washizu variational principle, the essential boundary condition enforcement has a similar form with the conventional Nitsche's method; both have consistent and stabilized terms. The costly high order derivatives in the Nitsche's consistent term have been replaced by the smoothed gradients, which improved the computational speed due to the reproducing kernel gradient smoothing framework. Furthermore, the stabilized term naturally existed in the Hu-Washizu weak form, and the artificial parameter needed in Nitsche's stabilized term has vanished, which can automatically maintain the coercivity for the stiffness matrix. The numerical results demonstrated that the proposed Hu-Washizu quasi-consistent meshfree thin shell formulation showed excellent accuracy, efficiency, and stability.

Acknowledgment

The support of this work by the National Natural Science Foundation of China (12102138, 52350410467) and the Natural Science Foundation of Fujian Province of China (2023J01108, 2022J05056) is gratefully acknowledged.

416 Appendix A. Green's theorems for in-plane vector

417 This Appendix discusses two kinds of Green's theorems used for the devel-
 418 opment of the proposed meshfree method. For an arbitrary vectors v^α and a
 419 scalar function f , with Green's theorem for in-plane vector, the first Green's
 420 theorem is listed as follows [30]:

$$\begin{aligned} \int_{\Omega} f_{,\alpha} v^\alpha d\Omega &= \int_{\Gamma} f v^\alpha n_\alpha d\Gamma - \int_{\Omega} f (v_{,\alpha}^\alpha + \Gamma_{\beta\alpha}^\beta v^\alpha) d\Omega \\ &= \int_{\Gamma} f v^\alpha n_\alpha d\Gamma - \int_{\Omega} f v^\alpha|_\alpha d\Omega \end{aligned} \quad (\text{A.1})$$

421 where $\Gamma_{\alpha\beta}^\gamma = \mathbf{a}_{\alpha,\beta} \cdot \mathbf{a}^\gamma$ denotes the Christoffel symbol of the second kind. $v^\alpha|_\alpha$
 422 can be represented as the in-plane covariant derivative of the vector v^α :

$$v^\alpha|_\alpha = v_{,\alpha}^\alpha + \Gamma_{\beta\alpha}^\beta v^\alpha \quad (\text{A.2})$$

423 The second Green's theorem is established with a mixed form of second
 424 order derivative. Let $A^{\alpha\beta}$ can be an arbitrary symmetric second order tensor,
 425 the Green's theorem yields [30]:

$$\begin{aligned} \int_{\Omega} f_{,\alpha}|_\beta A^{\alpha\beta} d\Omega &= \int_{\Gamma} f_{,\gamma} n^\gamma A^{\alpha\beta} n_\alpha n_\beta d\Gamma - \int_{\Gamma} f (A^{\alpha\beta} s_\alpha n_\beta)_{,\gamma} s^\gamma d\Gamma + [[f A^{\alpha\beta} s_\alpha n_\beta]]_{\mathbf{x} \in C} \\ &\quad - \int_{\Gamma} f (A_{,\beta}^{\alpha\beta} n_\alpha + \Gamma_{\alpha\beta}^\gamma A^{\alpha\beta} n_\gamma + \Gamma_{\gamma\beta}^\gamma A^{\alpha\beta} n_\alpha) d\Gamma \\ &\quad + \int_{\Omega} f \left(\Gamma_{\alpha\beta,\gamma}^\gamma A^{\alpha\beta} + \Gamma_{\alpha\beta}^\gamma A_{,\gamma}^{\alpha\beta} + \Gamma_{\eta\gamma}^\eta \Gamma_{\alpha\beta}^\gamma A^{\alpha\beta} \right. \\ &\quad \left. + A_{,\alpha\beta}^{\alpha\beta} + \Gamma_{\gamma\beta,\alpha}^\gamma A^{\alpha\beta} + 2\Gamma_{\gamma\alpha}^\gamma A_{,\beta}^{\alpha\beta} + \Gamma_{\gamma\alpha}^\gamma \Gamma_{\eta\beta}^\eta A^{\alpha\beta} \right) d\Omega \\ &= \int_{\Gamma} f_{,\gamma} n^\gamma A^{\alpha\beta} n_\alpha n_\beta d\Gamma - \int_{\Gamma} f (A^{\alpha\beta} s_\alpha n_\beta)_{,\gamma} s^\gamma d\Gamma + [[f A^{\alpha\beta} s_\alpha n_\beta]]_{\mathbf{x} \in C} \\ &\quad - \int_{\Gamma} f A^{\alpha\beta}|_\beta n_\alpha d\Gamma + \int_{\Omega} f A^{\alpha\beta}|_{\alpha\beta} d\Omega \end{aligned} \quad (\text{A.3})$$

426 with

$$A^{\alpha\beta}|_\beta = A_{,\beta}^{\alpha\beta} + \Gamma_{\beta\gamma}^\alpha A^{\beta\gamma} + \Gamma_{\gamma\beta}^\gamma A^{\alpha\beta} \quad (\text{A.4})$$

$$\begin{aligned} A^{\alpha\beta}|_{\alpha\beta} &= \Gamma_{\alpha\beta,\gamma}^\gamma A^{\alpha\beta} + \Gamma_{\alpha\beta}^\gamma A_{,\gamma}^{\alpha\beta} + \Gamma_{\eta\gamma}^\eta \Gamma_{\alpha\beta}^\gamma A^{\alpha\beta} \\ &\quad + A_{,\alpha\beta}^{\alpha\beta} + \Gamma_{\gamma\beta,\alpha}^\gamma A^{\alpha\beta} + 2\Gamma_{\gamma\alpha}^\gamma A_{,\beta}^{\alpha\beta} + \Gamma_{\gamma\alpha}^\gamma \Gamma_{\eta\beta}^\eta A^{\alpha\beta} \end{aligned} \quad (\text{A.5})$$

428 For the sake of brevity, the notion of covariant derivative is extended to a
 429 scalar function as:

$$f|_\alpha = f_{,\alpha} + \Gamma_{\beta\alpha}^\beta f \quad (\text{A.6})$$

$$f|_\beta n_\alpha = f_{,\beta} n_\alpha + \Gamma_{\alpha\beta}^\gamma f n_\gamma + \Gamma_{\gamma\beta}^\gamma f n_\alpha \quad (\text{A.7})$$

$$\begin{aligned} f|_{\alpha\beta} &= \Gamma_{\alpha\beta,\gamma}^\gamma f + \Gamma_{\alpha\beta}^\gamma f_{,\gamma} + \Gamma_{\eta\gamma}^\eta \Gamma_{\alpha\beta}^\gamma f \\ &\quad + f_{,\alpha\beta} + \Gamma_{\gamma\beta,\alpha}^\gamma f + 2\Gamma_{\gamma\alpha}^\gamma f_{,\beta} + \Gamma_{\gamma\alpha}^\gamma \Gamma_{\eta\beta}^\eta f \end{aligned} \quad (\text{A.8})$$

432 Appendix B. Derivations for stiffness metrics and force vectors

433 This Appendix details the derivations of stiffness matrices and force vectors
 434 in Eqs. (53)-(55), where the relationships of Eqs. (40), (41), (44) and (46) are
 435 used herein. Firstly, the membrane strain terms are considered as follows:

$$\begin{aligned}
 & \sum_{C=1}^{n_e} \int_{\Omega_C} \delta \tilde{\varepsilon}_{\alpha\beta}^h h C^{\alpha\beta\gamma\eta} \tilde{\varepsilon}_{\gamma\eta}^h d\Omega \\
 &= \sum_{C=1}^{n_e} \sum_{I,J=1}^{n_p} \delta \mathbf{d}_I \cdot \underbrace{\int_{\Omega_C} \tilde{\varepsilon}_{\alpha\beta I} h C^{\alpha\beta\gamma\eta} \mathbf{a}_\gamma \mathbf{q}^T d\Omega \mathbf{G}^{-1} \bar{\mathbf{g}}_{\eta J}}_{\tilde{\mathbf{g}}_I^{\eta T}} \cdot \mathbf{d}_J \\
 &= \sum_{C=1}^{n_e} \sum_{I,J=1}^{n_p} \delta \mathbf{d}_I \cdot \int_{\Gamma_C \cap \Gamma_v} \Psi_J \mathbf{q}^T \underbrace{\mathbf{G}^{-1} \tilde{\mathbf{g}}_I^\alpha n_\alpha}_{\tilde{\mathbf{T}}_{NI}} d\Gamma \cdot \mathbf{d}_J \\
 &= \sum_{I,J=1}^{n_p} \delta \mathbf{d}_I \cdot \int_{\Gamma_v} \tilde{\mathbf{T}}_{NI} \Psi_J d\Gamma \cdot \mathbf{d}_J
 \end{aligned} \tag{B.1}$$

436 with

$$437 \quad \tilde{\mathbf{g}}_I^\alpha = \mathbf{q} \mathbf{a}_\beta h C^{\alpha\beta\gamma\eta} \tilde{\varepsilon}_{\alpha\beta I} \tag{B.2}$$

$$438 \quad \tilde{\mathbf{T}}_{NI} = \mathbf{q}^T \mathbf{G}^{-1} \tilde{\mathbf{g}}_I^\alpha n_\alpha \tag{B.3}$$

Following this path, the bending strain terms can be reorganized by:

$$\begin{aligned}
 & \sum_{C=1}^{n_e} \int_{\Omega_C} \delta \tilde{\kappa}_{\alpha\beta}^h \frac{h^3}{12} C^{\alpha\beta\gamma\eta} \tilde{\kappa}_{\gamma\eta}^h d\Omega \\
 &= \sum_{C=1}^{n_e} \sum_{I,J=1}^{n_p} \delta \mathbf{d}_I \cdot \underbrace{\int_{\Omega_C} \tilde{\kappa}_{\alpha\beta I} \frac{h^3}{12} C^{\alpha\beta\gamma\eta} \mathbf{a}_3 \mathbf{q}^T d\Omega \mathbf{G}^{-1} \bar{\mathbf{g}}_{\gamma\eta J}}_{\tilde{\mathbf{g}}_I^{\gamma\eta T}} \cdot \mathbf{d}_J \\
 &= \sum_{C=1}^{n_e} \sum_{I,J=1}^{n_p} \delta \mathbf{d}_I \cdot \left(\begin{aligned} & \int_{\Gamma_C \cap \Gamma_\theta} \underbrace{\mathbf{q}^T \mathbf{G}^{-1} \tilde{\mathbf{g}}_I^{\alpha\beta} n_\alpha n_\beta}_{\tilde{\mathbf{M}}_{nnI}} n^\gamma \Psi_{J,\gamma} d\Gamma \\ & - \int_{\Gamma_C \cap \Gamma_v} \underbrace{(\mathbf{q}_{|\beta}^T \mathbf{G}^{-1} \tilde{\mathbf{g}}_I^{\alpha\beta} n_\alpha + (\mathbf{q}^T \mathbf{G}^{-1} \tilde{\mathbf{g}}_I^{\alpha\beta} s_\alpha n_\beta)_{,\gamma} s^\gamma)}_{\tilde{\mathbf{T}}_{MI}} \Psi_J d\Gamma \\ & + \underbrace{[\mathbf{q}^T \mathbf{G}^{-1} \tilde{\mathbf{g}}_I^{\alpha\beta} s_\alpha n_\beta \Psi_J]}_{\tilde{\mathbf{P}}_I \mathbf{a}_3} \Big|_{\mathbf{x} \in C_C \cap C_v} \end{aligned} \right) \cdot \mathbf{d}_J \\
 &= \sum_{I,J=1}^{n_p} \delta \mathbf{d}_I \cdot \left(\int_{\Gamma_\theta} \tilde{\mathbf{M}}_{nnI} n^\gamma \Psi_{J,\gamma} d\Gamma - \int_{\Gamma_v} \tilde{\mathbf{T}}_{MI} \Psi_J d\Gamma + [[\tilde{\mathbf{P}}_I \Psi_J]]_{\mathbf{x} \in C_v} \right)
 \end{aligned} \tag{B.4}$$

439 with

$$\tilde{\mathbf{g}}_I^{\alpha\beta} = \int_{\Omega_C} \mathbf{q} \frac{h^3}{12} C^{\alpha\beta\gamma\eta} \mathbf{a}_3 \tilde{\kappa}_{\alpha\beta I} d\Omega \quad (\text{B.5})$$

440

$$\begin{cases} \tilde{M}_{nnI} = \mathbf{q}^T \mathbf{G}^{-1} \tilde{\mathbf{g}}_I^{\alpha\beta} n_\alpha n_\beta \\ \tilde{\mathbf{T}}_{MI} = \mathbf{q}_{|\beta}^T \mathbf{G}^{-1} \tilde{\mathbf{g}}_I^{\alpha\beta} n_\alpha + (\mathbf{q}^T \mathbf{G}^{-1} \tilde{\mathbf{g}}_I^{\alpha\beta} s_\alpha n_\beta)_{,\gamma} s^\gamma \\ \tilde{\mathbf{P}}_I = \mathbf{q}^T \mathbf{G}^{-1} \tilde{\mathbf{g}}_I^{\alpha\beta} s_\alpha n_\beta \cdot \mathbf{a}_3 \end{cases} \quad (\text{B.6})$$

441 References

- 442 [1] L. H. Donnell, Beams, Plates and Shells, McGraw-Hill. `arXiv:0_`
443 `IeAQAAIAAJ`.
- 444 [2] T. J. Hughes, The Finite Element Method: Linear Static and Dynamic
445 Finite Element Analysis, Dover Publications.
- 446 [3] T. Belytschko, Y. Y. Lu, L. Gu, Element-free Galerkin methods 37 (2)
447 229–256. `arXiv:10208278`.
- 448 [4] W. K. Liu, S. Jun, Y. F. Zhang, Reproducing kernel particle methods
449 20 (8-9) 1081–1106.
- 450 [5] J. S. Chen, M. Hillman, S. W. Chi, Meshfree methods: Progress made after
451 20 years 143 (4) 04017001.
- 452 [6] P. Krysl, T. Belytschko, Analysis of thin shells by the Element-Free
453 Galerkin method 33 (20) 3057–3080.
- 454 [7] G. R. Liu, Meshfree Methods: Moving Beyond the Finite Element Method,
455 Second Edition, Crc Press.
- 456 [8] X. Zhang, K. Z. Song, M. W. Lu, X. Liu, Meshless methods based on
457 collocation with radial basis functions 26 333–343.
- 458 [9] D. Millán, A. Rosolen, M. Arroyo, Thin shell analysis from scattered points
459 with maximum-entropy approximants 85 (6) 723–751.
- 460 [10] L. Wang, M. Hu, Z. Zhong, F. Yang, Stabilized Lagrange Interpolation
461 Collocation Method: A meshfree method incorporating the advantages of
462 finite element method 404 115780.
- 463 [11] P. Suchde, T. Jacquemin, O. Davydov, Point Cloud Generation for Mesh-
464 free Methods: An Overview 30 (2) 889–915.
- 465 [12] L. Deng, D. Wang, An accuracy analysis framework for meshfree collocation
466 methods with particular emphasis on boundary effects 404 115782.
- 467 [13] S. Fernández-Méndez, A. Huerta, Imposing essential boundary conditions
468 in mesh-free methods 193 (12-14) 1257–1275.
- 469 [14] X. Li, Error estimates for the moving least-square approximation and the
470 element-free Galerkin method in n-dimensional spaces 99 77–97.
- 471 [15] J. Wu, D. Wang, An accuracy analysis of Galerkin meshfree methods ac-
472 counting for numerical integration 375 113631.
- 473 [16] J.-S. Chen, H.-P. Wang, New boundary condition treatments in meshfree
474 computation of contact problems 187 (3) 441–468.

- 475 [17] D. Liu, Y. M. Cheng, The interpolating element-free Galerkin (IEFG)
476 method for three-dimensional potential problems 108 115–123.
- 477 [18] V. Ivannikov, C. Tiago, P. M. Pimenta, On the boundary conditions of the
478 geometrically nonlinear Kirchhoff–Love shell theory 51 (18) 3101–3112.
- 479 [19] Y. Y. Lu, T. Belytschko, L. Gu, A new implementation of the element free
480 Galerkin method 113 (3-4) 397–414. [arXiv:26071039](#).
- 481 [20] T. Zhu, S. N. Atluri, A modified collocation method and a penalty formu-
482 lation for enforcing the essential boundary conditions in the element free
483 Galerkin method 21 (3) 211–222.
- 484 [21] S. Skatulla, C. Sansour, Essential boundary conditions in meshfree methods
485 via a modified variational principle: Applications to shell computations
486 15 (2) 123–142.
- 487 [22] J. S. Chen, C. T. Wu, S. Yoon, Y. You, A stabilized conforming nodal
488 integration for Galerkin mesh-free methods 50 (2) 435–466.
- 489 [23] J. S. Chen, M. Hillman, M. Rüter, An arbitrary order variationally con-
490 sistent integration for Galerkin meshfree methods 95 (5) 387–418. [arXiv:](#)
491 [260949200001](#).
- 492 [24] Q. Duan, X. Li, H. Zhang, T. Belytschko, Second-order accurate derivatives
493 and integration schemes for meshfree methods 92 (4) 399–424. [arXiv:](#)
494 [260949200001](#).
- 495 [25] D. Wang, J. Wu, An inherently consistent reproducing kernel gradient
496 smoothing framework toward efficient Galerkin meshfree formulation with
497 explicit quadrature 349 628–672.
- 498 [26] J. Wang, X. Ren, A consistent projection integration for Galerkin meshfree
499 methods 414 116143.
- 500 [27] J. Wu, X. Wu, Y. Zhao, D. Wang, A consistent and efficient method for
501 imposing meshfree essential boundary conditions via hellinger-reissner vari-
502 ational principle. 54 (12) 3283–3296.
- 503 [28] J. Wu, X. Wu, Y. Zhao, D. Wang, A rotation-free Hellinger-Reissner mesh-
504 free thin plate formulation naturally accommodating essential boundary
505 conditions 154 122–140.
- 506 [29] H. Dah-wei, A method for establishing generalized variational principle
507 6 (6) 501–509.
- 508 [30] J. Benzaken, J. A. Evans, S. F. McCormick, R. Tamstorf, Nitsche’s method
509 for linear Kirchhoff–Love shells: Formulation, error analysis, and verifica-
510 tion 374 113544.

- 511 [31] H. Du, J. Wu, D. Wang, J. Chen, A unified reproducing kernel gradient
512 smoothing Galerkin meshfree approach to strain gradient elasticity 70 (1)
513 73–100.
- 514 [32] R. H. Macneal, R. L. Harder, A proposed standard set of problems to test
515 finite element accuracy 1 (1) 3–20.